J. Fluid Mech. (1979), *vol.* 94, *part* 1, *pp.* 163–194
Printed in Great Britain

A test field model study of a passive scalar in isotropic turbulence

By GARY R. NEWMAN

Dept. of Mechanical Engineering, Southeastern Massachusetts University, North Dartmouth, Massachusetts 02747

AND JACKSON R. HERRING

National Center for Atmospheric Research, Boulder, Colorado 80307

(Received 6 October 1978)

This paper applies the test field model developed by Kraichnan to the study of an isotropic, passive scalar contaminant convected by decaying isotropic turbulence. Test field model predictions of scalar and velocity dissipation spectra at large Reynolds and Péclet numbers are shown to be in excellent agreement with atmospheric data, after intrinsic scale constants in the model are adjusted to give valid inertial range coefficients. Theoretical values for the inertial range coefficients are obtained for large and small Prandtl numbers. Simulation results for velocity and scalar energy, dissipation and transfer spectra and second- and third-order velocity, scalar and velocity–scalar correlations at moderate Reynolds and Péclet numbers are shown to agree moderately well with heated grid turbulence data. Simulation results are presented for the normalized decay rates of the scalar and velocity dissipation rates and for the ratio of the velocity to scalar decay time scales; these quantities are employed in second-order modelling. In the self-similar decay mode the simulations yield unity levels of the normalized decay rates and of the ratio of decay time scales over the moderate range of Reynolds and Prandtl numbers investigated. These results are compared with data from heated grid turbulence experiments and are discussed in the light of asymptotic decay of concomitant scalar and velocity fields.

1. Introduction

This paper applies the test field model (TFM) (Kraichnan 1971) to the study of an isotropic, passive scalar contaminant convected by decaying isotropic turbulence. Our motivation is twofold; first, to ascertain the accuracy of the theory by a comparison of its predictions to experiments at both moderate and large Reynolds and Péclet numbers, and second, to extract from self-similar decay studies certain normalized decay rates of use in single point closures (Lumley 1970; Lumley & Newman 1977). We compare the theory's predictions to both the moderate Reynolds number ($R_\lambda \simeq 35$) experiments of Yeh & Van Atta (1973) and to the large Reynolds number atmospheric measurements of Champagne *et al.* (1977). The comparison includes an analysis which yields theoretical values for the inertial range coefficients for large and small Prandtl numbers, as well as one-dimensional spectral profiles in the dissipation range. The normalized decay rates obtained for self-similar decay include those

0022–1120/79/4251–7020 $02.00

coefficients relating the decay rate of dissipation to dissipation and energy for both the velocity and scalar fields.

Section 2 records the TFM equations for the velocity and the scalar fields. The prescription is taken from Kraichnan (1971); the velocity field equations are recorded there, and at the end of this section is stated a prescription for the scalar field. The latter represents a Markovian scalar theory in which the time scale for the scalar variance is the time scale of the test field's compressive component. A brief development of the scalar TFM and a discussion of its consistency properties are presented in the appendix.

Section 3 gives the comparison of theory and experiments of Yeh & Van Atta (1973) for moderate Reynolds number ($R_\lambda \simeq 35$). The comparison includes energy and dissipation spectra, transfer functions, and second- and third-order velocity–temperature correlations. Section 4 contains an examination of the predictions of theory for very large Reynolds number flows. We include here a determination of the scalar inertial range coefficient, as well as a comparison of dissipation spectra to the data of Champagne *et al.* (1977). Finally, § 5 discusses the predictions of the TFM for the normalized decay rates, $\psi \equiv \epsilon q^2/\epsilon^2$ and $\psi_\theta \equiv \epsilon_\theta \overline{\theta^2}/\epsilon_\theta^2$, and for the ratio of velocity to scalar decay time scales, $r \equiv (\overline{q^2}/\epsilon)/(\overline{\theta^2}/\epsilon_\theta)$, which are employed in single-point closures. Here, ϵ and ϵ_θ are dissipation of kinetic energy ($= \frac{1}{2}\overline{q^2}$) and one half of the scalar variance ($= \overline{\theta^2}$); i.e.

$$\epsilon = \nu \overline{\frac{\partial u_i}{\partial x_j}\frac{\partial u_i}{\partial x_j}} \quad \text{and} \quad \epsilon_\theta = \gamma \overline{\frac{\partial \theta}{\partial x_i}\frac{\partial \theta}{\partial x_i}},$$

where ν and γ are respectively the velocity and scalar molecular diffusivities.

The results of this investigation indicate the TFM to be in good agreement with the large Reynolds number observations, but in only moderate agreement with the $R_\lambda \simeq 35$ data of Yeh & Van Atta (1973). At large Reynolds number, we obtain excellent agreement with the observations of Champagne *et al.* (1977) for both scalar and velocity dissipation functions, provided the empirical constants of the TFM are adjusted to give valid inertial range coefficients. With regard to the disagreement with the data of Yeh & Van Atta, we tentatively conclude that the TFM has certain inadequacies apparent at moderate Reynolds number which are not explicit at very large R_λ. A comparison of accurate numerical simulation with theory is needed here to accurately fix theoretical errors. Values of the velocity and scalar dissipation rates computed for self-similar decay at small and moderate R_λ are approximately 4·0. Also the ratio ψ/ψ_θ and the time scale ratio are approximately unity. The only unusual feature of the present calculations is that we find no evidence in the TFM for a final period of decay.

2. Theory

Kinematical considerations

Consider a passive scalar, $\theta(\mathbf{x}, t)$, convected by an incompressible velocity field, $\mathbf{v}(\mathbf{x}, t)$, whose statistical properties are homogeneous and isotropic. We seek governing equations for ensemble averages of the second-order moments of $(\mathbf{v}, \theta)$,

$$U_{ij}(\mathbf{x}, t; \mathbf{x}', t') = \langle v_i(\mathbf{x}, t)\, v_j(\mathbf{x}', t')\rangle, \tag{2.1}$$

$$\Theta(\mathbf{x}, t; \mathbf{x}', t') = \langle \theta(\mathbf{x}, t)\, \theta(\mathbf{x}', t')\rangle, \tag{2.2}$$

given the equations of motion for $(\mathbf{v}, \theta)$:

$$(\partial/\partial t + \mathbf{v}.\nabla)\,\mathbf{v} = -\nabla p - \nu\nabla^2\mathbf{v}, \tag{2.3}$$

and

$$(\partial/\partial t + \mathbf{v}.\nabla)\,\theta = -\gamma\nabla^2\theta. \tag{2.4}$$

The statistical turbulence theory is most conveniently formulated in terms of the spectral representation of (2.1) and (2.2). Accordingly, we decompose $(\mathbf{v}, \theta)$ into Fourier modes $(\mathbf{v}(\mathbf{k}), \theta(\mathbf{k}))$, defined by

$$(v_i(\mathbf{x}, t), \theta(\mathbf{x}, t)) = \sum_{\mathbf{k}} \exp(i\mathbf{k}.\mathbf{x})(v_i(\mathbf{k}, t), \theta(\mathbf{k}, t)).$$

Here, $\mathbf{k} = (\hat{\imath}n, \hat{\jmath}m, \hat{k}l)\,(2\pi/\mathscr{L})$, $(n, m, l) = (-\infty, \ldots, -1, 0, 1, 2, \ldots, \infty)$, and $\mathscr{L}$ is an arbitrary length much larger than any physically relevant length scale. Corresponding to the two-point moments (2.1) and (2.2) are the modal velocity and scalar variances spectra,

$$(U_{ij}(k, t, t'),\ \Theta(k, t, t')) = \int d(\mathbf{x}-\mathbf{x}) \exp(i\mathbf{k}.(\mathbf{x}-\mathbf{x}'))\,(U_{ij}(\mathbf{x}, \mathbf{x}'), \Theta(\mathbf{x}, \mathbf{x}')), \tag{2.5}$$

which are the principal ingredients of the statistical theory. We recall that, for isotropic turbulence,

$$U_{ij}(k, t, t') = \tfrac{1}{2}(\delta_{ij} - k_i k_j/k^2)\,U(k, t, t'), \tag{2.6}$$

where $U(k, t, t')$ is related to the kinetic energy spectrum by

$$E(k, t) = \tfrac{1}{2}(4\pi k^2)\,U(k, t, t). \tag{2.7}$$

We define an analogous θ-energy by

$$E_\theta(k, t) = \tfrac{1}{2}(4\pi k^2)\,\Theta(k, t, t). \tag{2.8}$$

The total kinetic energy per unit mass is then

$$\tfrac{1}{2}\overline{q^2} = \tfrac{1}{2}\langle \mathbf{v}^2(\mathbf{x}, t)\rangle = \int_0^\infty dk\,E(k, t), \tag{2.9}$$

and similarly

$$\tfrac{1}{2}\langle \theta^2(\mathbf{x}, t)\rangle = \int_0^\infty dk\,E_\theta(k, t). \tag{2.10}$$

In (2.9), and hereafter, we denote by $(\overline{q^2})^{\frac{1}{2}}$ the volume-average r.m.s. speed, which for homogeneous flows is identical to the ensemble r.m.s. average of $\mathbf{v}$. We record here for subsequent reference the one-dimensional velocity and scalar spectra:

$$\Phi_v(k_1) = \frac{1}{2}\int_{k_1}^\infty dp\,(1 - k_1^2/p^2)\,E(p)/p, \tag{2.11}$$

$$\Phi_\Theta(k_1) = \int_{k_1}^\infty dp\,E_\theta(p)/p, \tag{2.12}$$

and note that, in terms of these one-dimensional spectra,

$$\overline{q^2} = \langle \mathbf{v}^2\rangle = \int_{-\infty}^\infty dk_1\,\phi_v(k_1) = (2)\int_0^\infty dk\,E(k), \tag{2.13}$$

$$\overline{\theta^2} = \langle \theta^2\rangle = \int_{-\infty}^\infty dk_1\,\phi_\theta(k_1) = 2\int_0^\infty dk\,E_\theta(k). \tag{2.14}$$

Further, the dissipation of kinetic energy and θ-energy are

$$-\tfrac{1}{2}\dot{\overline{q^2}} = -\nu\langle \mathbf{v}.(\nabla^2\mathbf{v})\rangle = 15\nu\int_{-\infty}^{\infty} k_1^2\, dk_1\, \phi_v(k_1) = 2\nu\int_0^{\infty} dk\, E(k)\, k^2 = \epsilon, \tag{2.15}$$

$$-\tfrac{1}{2}\dot{\overline{\theta^2}} = -\gamma\langle \theta\nabla^2\theta\rangle = 3\gamma\int_{-\infty}^{\infty} k_1^2\, dk_1\, \phi_\theta(k_1) = 2\gamma\int_0^{\infty} dk\, E_\theta(k)\, k^2 = \epsilon_\theta. \tag{2.16}$$

The test field model (TFM)

The test field model (TFM) for $U(k,t,t')$ is (Kraichnan 1971)

$$(\partial/\partial t + \nu k^2 + \eta_v(k))\, U(k,t,t') = 0 \quad (t \neq t'), \tag{2.17}$$

$$(\tfrac{1}{2}d/dt + \nu k^2)\, U(k,t,t) = \int_\Delta dp\, dq\, B(k,p,q)\, D(k,p,q)\, (U(p,t,t) - U(k,t,t)\, U(q,t,t), \tag{2.18}$$

where
$$B(k,p,q) = \pi \sin^2(p,q)\, ((p^2-q^2)\,(k^2-q^2) + p^2 k^2)\, pq/k^3, \tag{2.19}$$

$$dD(k,p,q)/dt = 1 - (\eta^s(k) + \eta^s(p) + \eta^s(q) + \nu(k^2+p^2+q^2))\, D(k,p,q),$$

with
$$D(k,p,q|t=0) = 0, \tag{2.20}$$

$$\eta^s(k) = g^2\int_\Delta C(k,p,q)\, D^s(k,p,q)\, U(q)\, dp\, dq, \tag{2.21}$$

$$\eta^c(k) = 2g^2\int_\Delta C(k,p,q)\, D^c(k,p,q)\, U(q)\, dp\, dq, \tag{2.22}$$

$$dD^s(k,p,q)/dt = 1 - (\eta^s(k) + \eta^c(p) + \eta^s(q) + \nu(k^2+p^2+q^2))\, D^s(k,p,q),$$

with
$$D^s(k,p,q|t=0) = 0, \tag{2.23}$$

$$\left.\begin{aligned} dD^c(k,p,q)/dt &= 1 - (\eta^c(k) + \eta^s(p) + \eta^s(q) + \nu(k^2+p^2+q^2))\, D^c(k,p,q), \\ D^c(k,p,q|t=0) &= 0, \end{aligned}\right\} \tag{2.24}$$

and
$$C(k,p,q) = \tfrac{1}{2}\pi kpq \sin^2(k,p) \sin^2(k,q). \tag{2.25}$$

In (2.18), (2.21) and (2.22), the integrals over $(dp\,dq)$ extend over all (p,q) such that (k,p,q) can form a triangle ($\mathbf{k} = \mathbf{p}+q$). Zero initial values for D, D^s and D^c signify that the initial statistics of $\mathbf{v}$ are multivariate Gaussian.

The key equation here is (2.18). Its right-hand side consists of an input term, which gives the change of $U(k)$ from other modes ($\mathbf{p}, \mathbf{q}$), and an output term, which gives the drain on mode $\mathbf{k}$ because of its interaction with other modes, $\mathbf{q}$. The coefficient, $B(k,p,q)$ [(2.19)] stems from the non-linearity of the Navier–Stokes equation (2.3). The formal structure of (2.18) is quite similar to the quasi-normal approximation; to obtain the latter, we need only replace $D(k,p,q)\,(U(p,t)\,U(q,t) - U(k,t)\,U(q,t))$ by $\int_0^t ds\,(U(p,s)\,U(q,s) - U(k,s)\,U(q,s))$, suppressing for the moment the viscous dissipation. The time scale $D(k,p,q)$ may be thought of as the mean duration of the distortion process, which changes energy in mode k. Physically, it is the r.m.s. strain by scales larger than $2\pi/k$. Mathematically, (2.20)–(2.25) give evolution equations for the triple moment time scale $D(k,p,q)$. Their basic ingredients are two relaxation rates, $\eta^s(k)$, and $\eta^c(k)$, which pertain to a test field which suffers pure convection (no pressure

forces) by $\mathbf{v}(\mathbf{x}, t)$. $\eta^s(k)$ gives the rate at which interactions with $\mathbf{v}(\mathbf{x}, t)$ induce solenoidal components of the test field to be converted into the compressive mode, while $\eta^c(k)$ gives the rate at which such an interaction induces the compressive mode to be transformed into solenoidal modes. The empirical parameter, g, in (2.21) and (2.22) gives the efficacity of the above algorithm in distorting fluid elements. It may be fixed by comparing the inertial range prediction of the TFM to experiment

$$(E(k) = 1{\cdot}34 g^{\frac{4}{3}} \epsilon^{\frac{2}{3}} / k^{\frac{5}{3}})$$

(Leith & Kraichnan 1972). The factor 2 in (2.22) stems from the fact that for isotropic turbulence there are two equivalent solenoidal modes, but only one compressive mode.

The basic idea behind the TFM is that it is the pressure force that limits the duration of straining of eddies of size $2\pi/k$. The time scale for such a distortion is measured by the effects of removing the pressure force; in other words, examining what the pressure force prevents.

The TFM constitutes a Markovian, modified perturbation expansion for the (second order) statistics of the Navier–Stokes equations. By this we mean that the nonlinear forces that produce Eulerian accelerations are modelled to zeroth order by white noise, and the parameters of the model force field are determined through an examination of a self-consistent perturbation theory. The white noise modelling explains why all time arguments in (2.18)–(2.25) refer to the current time, t. For further details, we refer the interested reader to Kraichnan (1971).

For the scalar field, $\Theta(k, t, t')$, the TFM employed here is

$$(\partial/\partial t + \gamma k^2 + \eta(k))\,\Theta(k,t,t') = 0 \quad (t \neq t'), \tag{2.26}$$

$$(\tfrac{1}{2}d/dt + \gamma k^2)\,\Theta(k,t,t) = \int_\Delta dp\,dq\,B^\theta(k,p,q)\,D^\theta(k,p,q)\,U(q,t,t)\,(\Theta(p,t,t) - \Theta(k,t,t)), \tag{2.27}$$

$$dD^\theta(k,p,q)/dt = 1 - (g_\theta^2(\eta^c(k) + \eta^c(p)) + \eta^s(q) + \gamma(k^2 + p^2) + \nu q^2)\,D^\theta(k,p,q),$$

where
$$D^\theta(k,p,q|t=0) = 0 \tag{2.28}$$

and
$$B^\theta(k,p,q) = \pi \sin^2(p,q)\,p^3 q/k. \tag{2.29}$$

The equation for $\eta(k, t)$ is (A 7) of the appendix, provided the triple moment relaxation factor in (A 7) (i.e.: $H(k,p,q)$) is replaced by $D^\theta(k,p,q)$ as given by (A 16). These equations are derived (see appendix) by an application of the Markovian, modified perturbation theory – cited above – to the scalar field, with the provision that the relaxation time for the scalar variance is $\eta^c(k) g_\theta$, where g_θ is an adjustable parameter for θ, in the same manner that g_v in (2.21) and (2.22) is for $\mathbf{v}$. Thus, we should adjust g_θ^2 so that $\phi_\theta(k_1)$, as given by (2.12), is $0{\cdot}4\chi\epsilon^{-\frac{1}{3}}k^{-\frac{5}{3}}$, if the theory is to be matched to experiments on Prandtl number unity fluids (Champagne *et al.* 1977). We postpone a full discussion of the large Reynolds number behaviour of this spectrum until § 4, and here only quote the value that gives acceptable values for ϕ_θ:

$$g_\theta = 0{\cdot}5, \tag{2.30}$$

$$g_v = 1{\cdot}5. \tag{2.31}$$

The identification of $\eta^c(k)$ as the time scale for the relaxation of the θ-field triple moments results from the fact that $\partial\theta/\partial x_i$ is the test field (rather than θ itself) upon which the TFM algorithm is to be applied.

3. Moderate Reynolds number results

Introduction

In this section we compare TFM simulation results with the experimental data of Yeh & Van Atta (1973) which pertains to scalar decay in grid turbulence. We shall compare energy, dissipation and transfer spectra as well as second and third-order velocity, scalar and velocity–scalar correlations. We noted above that the TFM prescriptions are augmented by the adjustable factors g_v and g_θ which provide a means of tuning the characteristic memory times which control the build-up of the triple moments. We shall determine values for these coefficients in § 4 by fitting theory predictions of one-dimensional scalar and velocity spectra to large Reynolds number (atmospheric) spectra in the inertial wavenumber range. We have utilized the values of g_v and g_θ given by the inertial range comparisons in the simulations presented here; we discuss briefly the implications of altering these values in § 6. Before presenting the data–theory comparisons, we first describe the numerical techniques and initial conditions employed in our TFM simulations.

With the TFM given above, we must solve prognostic equations for U, D, D^c, D^s, Θ and D^θ along with diagnostic equations for η^s and η^c. Our numerical integration procedures follow those of Herring & Kraichnan (1972). The wavenumber domain is discretized into an interpolating set, $\{k\}_{i=1}^{35}$, of 35 points which span $k \in [0, 100]$, and the $\{k\}_i$ are distributed with maximum point density at the low wavenumbers so as to provide good representations of velocity and scalar spectra. The continuous TFM equations are evaluated on this discrete set of wavenumbers, and the time stepping for the prognostic equations is performed with two-step predictor corrector marching on the set $\{k\}_i$. The p, q integrations in the model equations are effected by employing Gaussian quadrature on cubic spline representations of the integrands. As noted, the p–q integration domain spans allowed (p, q) such that (k, p, q) form a triangle ($\mathbf{k} = \mathbf{p} + \mathbf{q}$), and here the $(p$–$q)$ domain is truncated for a fixed k_i using the scheme of Herring & Kraichnan (1972) which guarantees energy conservation.

The initial states of the scalar and velocity fields in our simulations are represented by chosen forms for the three-dimensional spectra, $E(k, 0)$ and $E_\theta(k, 0)$, and by zero spectral transfer. The following form for the initial spectra (where H denotes either E or E_θ) was employed in the predictions discussed in this section:

$$H(K, 0) = Ake^{-k/B}, \quad A, B = \text{constant}. \tag{3.1}$$

The spectral form (3.1) evolves rapidly into spectra which are very nearly identically self-preserving. We shall further address the issue of initialization in § 6.

We may assess the overall accuracy of our numerical scheme by examining the energy balance equations for the velocity and scalar fields given above in (2.15) and (2.16). By numerically differentiating the data from our TFM simulations we find that the error quantities

$$|\dot{\overline{q^2}}/(2\epsilon) - 1|, \quad |\dot{\overline{\theta^2}}/(2\epsilon_\theta) - 1|, \tag{3.2}$$

are less than 1×10^{-3} at each step for all of our simulations. Our simulations cover a dimensional time range from 0·0 to a maximum of 3·0, and thus with the results (3.2) we deduce that the cumulative error growth in the balance equations is small.

Comparison with experiments

We now compare predictions with the heated grid turbulence data of Yeh & Van Atta (1973). We shall discuss their results in the light of recent work by Warhaft & Lumley (1978) in § 5. The scalar contaminant in the experiments of Yeh & Van Atta (1973) was temperature, and the thermal fluctuations were input into their laboratory flow by heating the grid which was employed to generate the turbulent flow field. The thermal fluctuations were relatively small so that buoyancy effects were negligible and hence the temperature contaminant behaved passively. Decaying heated grid turbulence is known to exhibit approximate isotropy of the flow fields and to exhibit approximate partial self-preservation of various turbulence quantities when the quantities are normalized with appropriate local variables. We shall compare normalized experimental and predicted spectra. However, after Herring & Kraichnan (1972), we note that it is difficult to assess to what extent the period of temporal evolution predicted in our simulations corresponds to that of the experiments. Our simulations march forward in time from chosen initial spectral forms, whereas the grid turbulence fields evolve from coalescing heated wakes (which are initiated behind the grid bars) and hence presumably have markedly different initial spectra. On the other hand, we compare approximately self-preserving forms of the simulation results and the data, and these results may well be fairly universal in nature.

To effect simulation of the Yeh & Van Atta (1973) flow, we have simply reproduced their value of Prandtl number ($\nu/\gamma = 0{\cdot}725$) and closely matched the values of R_λ (the turbulence Reynolds number) and P_λ which were exhibited in their flow at the mid-point tunnel position $x/M = 35$ (where M is the grid mesh size), where we define R_λ and P_λ as

$$R_\lambda = u^1\lambda/\nu, \quad P_\lambda = u^1\lambda_\theta/\gamma, \quad u^1 = (\overline{q^2}/3)^{\frac{1}{2}}, \tag{3.3}$$

λ and λ_θ are the velocity and the scalar Taylor microscales given by

$$\lambda = (5\nu\overline{q^2}/\epsilon)^{\frac{1}{2}} = \left(5\int_0^\infty E(k,t)\,dk \Big/ \int_0^\infty k^2E(k,t)\,dk\right)^{\frac{1}{2}}, \tag{3.4}$$

$$\lambda_\theta = (6\gamma\overline{\theta^2}/\epsilon_\theta)^{\frac{1}{2}} = \left(6\int_0^\infty E_\theta(k,t)\,dk \Big/ \int_0^\infty k^2E_\theta(k,t)\,dk\right)^{\frac{1}{2}}. \tag{3.5}$$

The values of (R_λ, P_λ) from Yeh & Van Atta (1973) are (35·2, 32·5) while the values from our simulation are (37·1, 32·7). These 'asymptotic' (R_λ, P_λ) simulation values correspond to a dimensional evolution time of 1·3, but we note that both R_λ and P_λ change very slowly with time in any TFM simulation after self-preservation is achieved.

In figures 1–12 we compare our simulation results with the data of Yeh & Van Atta (1973) for the following normalized quantities (where we now drop explicit time dependence): $E(k)$, $T(k) \equiv$ the three-dimensional velocity transfer spectrum, $k^2E(k) \equiv$ the three-dimensional velocity dissipation spectrum, $R(u, u) \equiv$ the double velocity correlation, $R(uu, u) \equiv$ the triple velocity correlation, $E_\theta(k)$, $T_\theta(k) \equiv$ the three-dimensional scalar transfer spectrum, $k^2E_\theta(k) \equiv$ the three-dimensional scalar dissipation spectrum, $R(\theta, \theta) \equiv$ the double scalar correlation and $R(u\theta, \theta) \equiv$ the triple velocity–scalar correlation. The defining relations for the transfer spectra and the double and triple correlations are given below. The simulation spectra presented

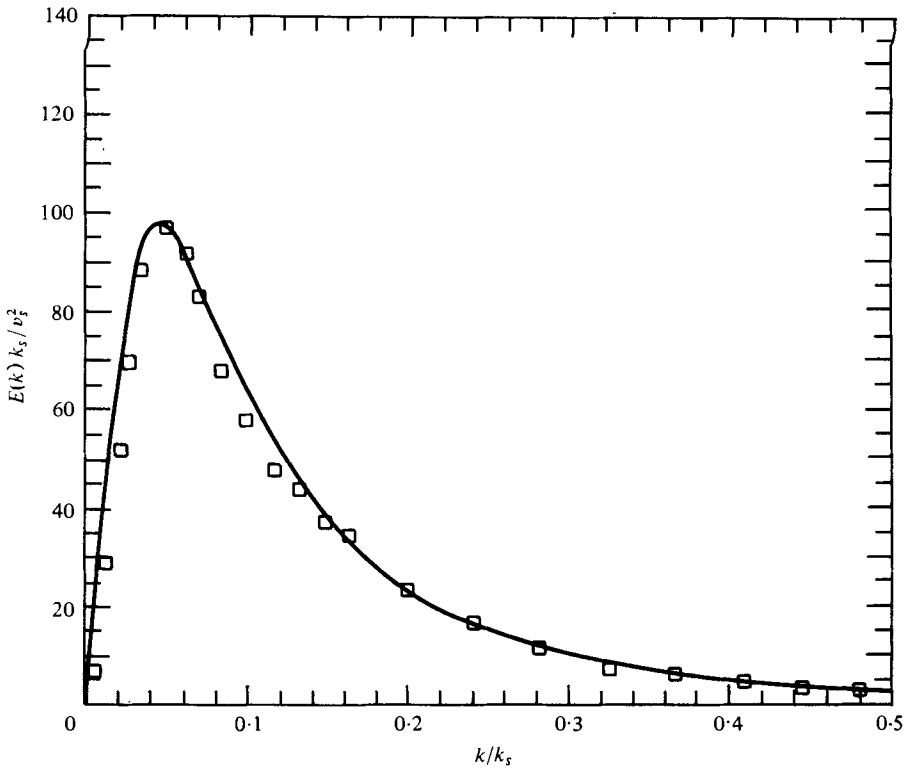

FIGURE 1. Normalized three-dimensional velocity energy spectra. ——, our TFM prediction; □, data of Yeh & Van Atta (1973).

correspond to a dimensional evolution time of $t = 1{\cdot}3$, however, they represent nearly universal shapes for all t such that self-preservation is closely maintained. The data spectra pertain to the mid-point tunnel position of $x/M = 35$. We utilize local values of $k_s \equiv (\epsilon/\nu^3)^{\frac{1}{4}}$ and $v_s \equiv (\epsilon\nu)^{\frac{1}{4}}$ (respectively, the inverse of the Kolmogorov length scale and the Kolmogorov velocity scale) to scale many of the spectra. This small scale normalization collapses the predicted spectra into nearly self-preserving forms over the entire range of wavenumbers; whereas the small scale normalization collapses only the high wavenumber regions of the data energy and transfer spectra. The data dissipation spectra collapse well over the whole wavenumber range however. The normalization of scalar spectral quantities with the velocity quantities k_s and v_s follows Yeh & Van Atta (1973). We note that this scaling is strictly valid only for the case of unity Prandtl number. For cases with significant departures from unity Prandtl number, scalar spectra must be normalized with scales relevant to the contaminant field. We have employed such scaling in our presentation of the scalar correlation quantities and of the large scale normalization of the scalar energy spectra.

Figures 1 and 2 show the data and predicted $E(k)$ spectra normalized, respectively, with small scale and large scale normalization, while figures 3 and 4 show the corresponding normalized $E_\theta(k)$ spectra. The large scale normalization employed serves to collapse the low wavenumber regions of the spectra. The agreement between theory and experiment is seen to be quite good for both $E(k)$ and $E_\theta(k)$ at low and high wavenumbers. The agreement at moderate wavenumbers is good for $E(k)$ and fair for $E_\theta(k)$.

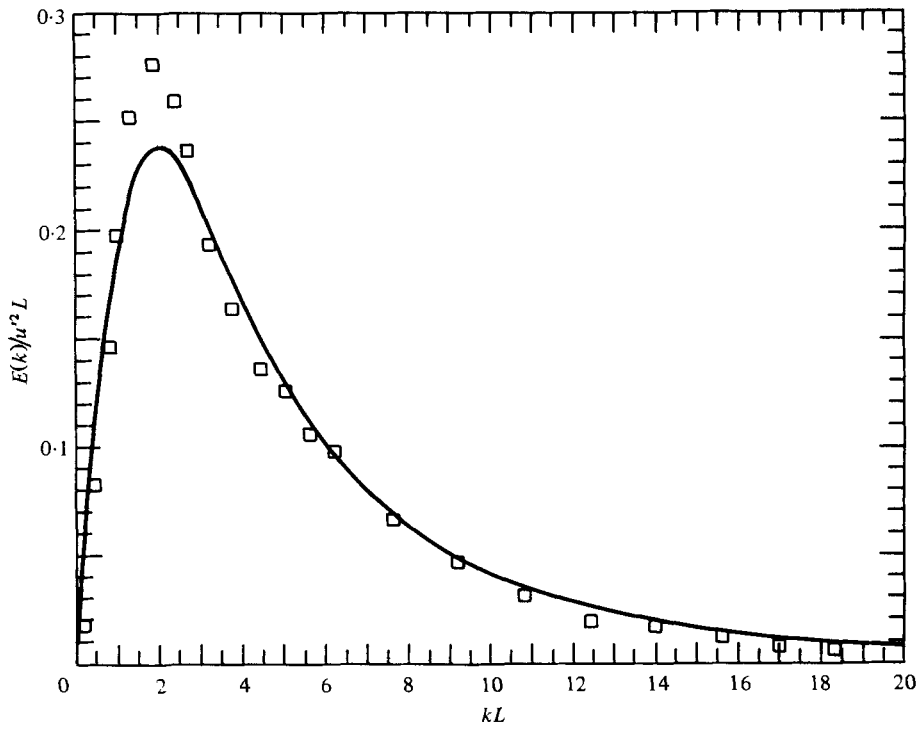

FIGURE 2. Normalized three-dimensional velocity energy spectra. ——, our TFM prediction; □, data of Yeh & Van Atta (1973).

We note that both the computed and empirical spectra exhibit the quality that $E_\theta(k)$ peaks at a lower wavenumber than $E(k)$, and we shall consider this behaviour further in § 5.

Figures 5 and 6 show, respectively, the three-dimensional velocity and scalar transfer spectra, $T(k)$ and $T_\theta(k)$, which we now define. $T(k)$ and $T_\theta(k)$ represent, respectively, the transfer of energy and scalar variance to wavenumber k from all other wavenumbers. The transfer spectra serve as forcing functions in the corresponding spectral balance equations for the three-dimensional energy spectra which we may write as

$$(d/dt + 2\nu k^2)\, E(k,t) = T(k,t), \tag{3.6}$$

$$(d/dt + 2\gamma k^2)\, E_\theta(k,t) = T_\theta(k,t). \tag{3.7}$$

We may form (3.6) and (3.7) from our TFM by multiplying (2.18) and (2.27) by $4\pi k^2$ so that $T(k)$ and $T_\theta(k)$ denote the product of $4\pi k^2$ and the nonlinear interaction terms on the right-hand sides of (2.18) and (2.27), respectively. The transfer spectra for the TFM may be shown to satisfy energy conservation by nonlinear interaction which is expressed by the relations

$$\int_0^\infty T(k)\, dk = \int_0^\infty T_\theta(k)\, dk = 0. \tag{3.8}$$

Relations (3.8) are satisfied by the transfer spectra associated with truncated-wavenumber representations of the scalar and velocity equations of motion for isotropic scalar turbulence.

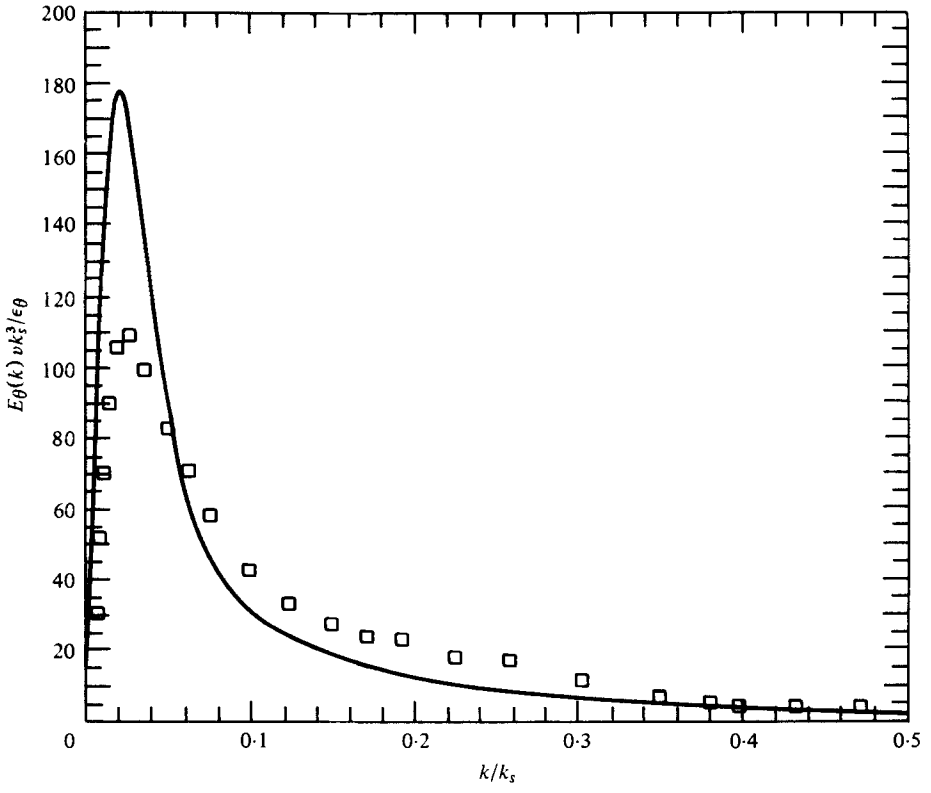

FIGURE 3. Normalized three-dimensional scalar energy spectra. ——, our TFM prediction; □, data of Yeh & Van Atta (1973).

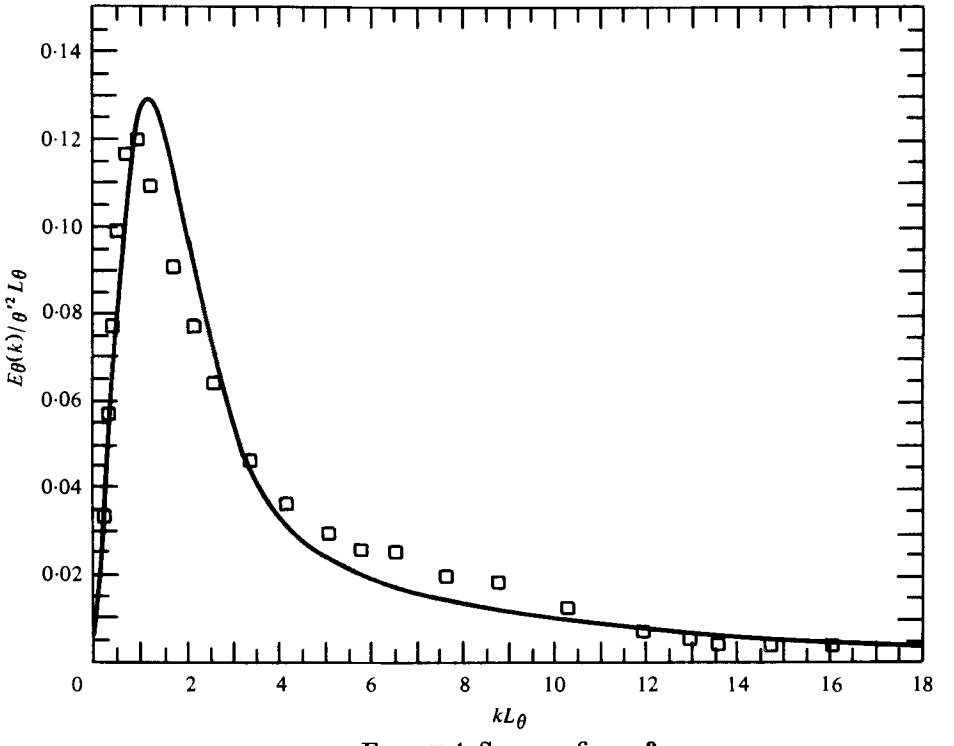

FIGURE 4. Same as figure 3.

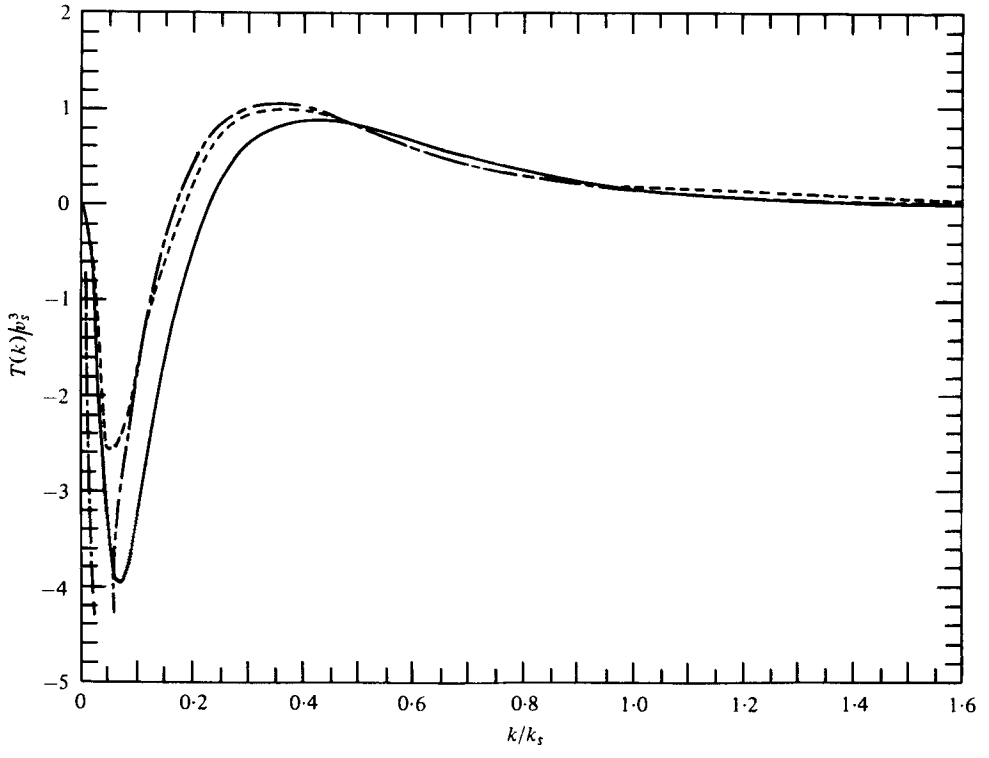

FIGURE 5. Normalized three-dimensional velocity transfer spectra. ——, our TFM prediction; —·—, Yeh & Van Atta (1973) directly measured data; – – – – –, Yeh & Van Atta (1973) spectral balance results.

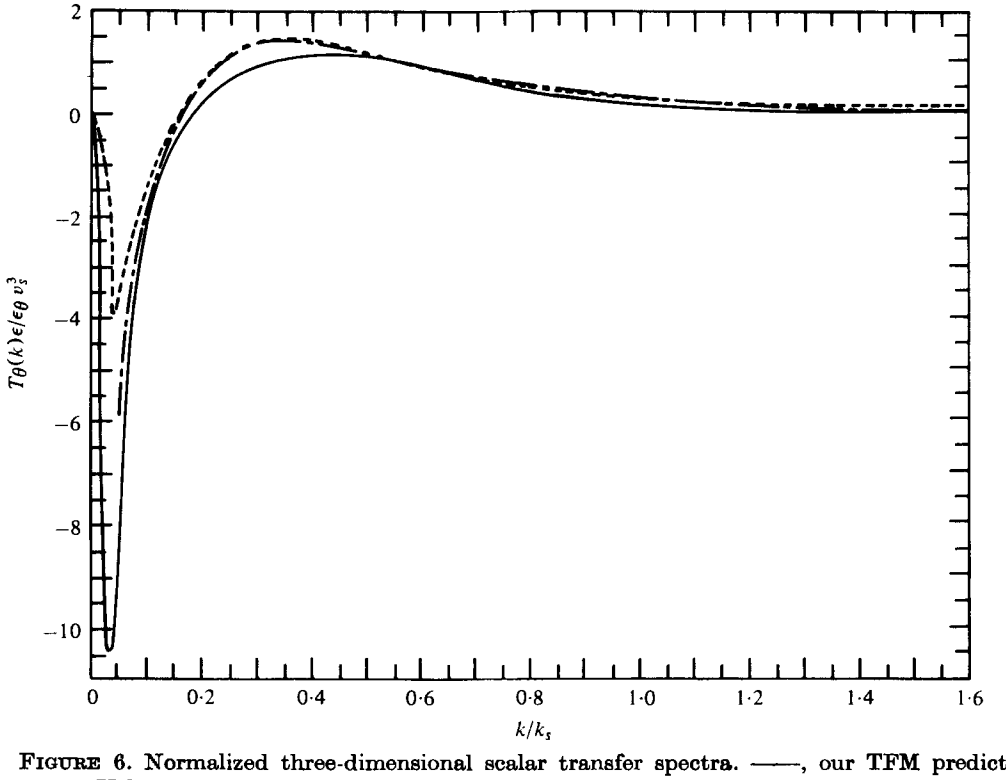

FIGURE 6. Normalized three-dimensional scalar transfer spectra. ——, our TFM prediction; —·—, Yeh & Van Atta (1973) directly measured data; – – – – –, Yeh & Van Atta (1973) spectral balance results.

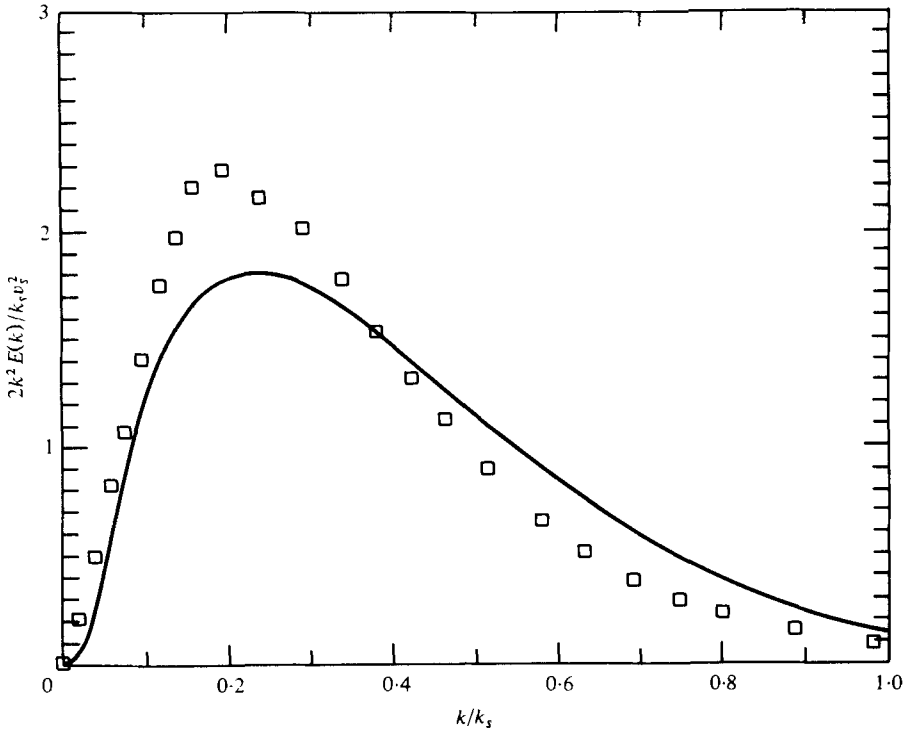

FIGURE 7. Normalized three-dimensional velocity dissipation spectra. ——, our TFM prediction; □, data of Yeh & Van Atta (1973).

From figures 5 and 6 we observe that the agreement between simulation and data profiles of $T(k)$ and $T_\theta(k)$ is good at the high wavenumbers. Agreement at the low wavenumbers is not as good, but direct comparison at these wavenumbers is not too enlightening since the low wavenumber portions of the data curves are presumably not self-preserving under the small scale normalization employed. In addition, as indicated in figures 5 and 6, Yeh & Van Atta (1973) could not accurately map the entire negative regions of $T(k)$ and $T_\theta(k)$ by direct measurements. We have included for comparison in the figures the profiles of $T(k)$ and $T_\theta(k)$ which they determined indirectly using the spectral balance equations (3.6) and (3.7). We note that Yeh & Van Atta (1973) indicate that the energy conservation properties (3.8) are not satisfied identically by their directly measured data. Curves with a positive area contribution exceed the negative area by 50 % for $T_\theta(k)$, while curves with a negative area contribution exceed the positive area by 10 % for $T(k)$.

The velocity and scalar dissipation spectra are shown in figures 7 and 8. The agreement between simulation and data is fair with $k^2E_\theta(k)$ somewhat better reproduced at high wavenumbers and $k^2E(k)$ somewhat better reproduced at the lower wavenumbers. The greatest disparities between theory and experiment occur in the region of the spectral peaks. On the other hand, we note that Yeh & Van Atta (1973) compare their velocity dissipation spectrum with spectra of Uberoi (1963) (with $R_\lambda \simeq 70$) and Van Atta & Chen (1969) (with $R_\lambda \simeq 35$). It can be seen from their comparison figure that the Uberoi (1963) values agree well with those of Yeh & Van Atta (1973) while the values of Van Atta & Chen (1969) are lower than those of Yeh & Van Atta (1973)

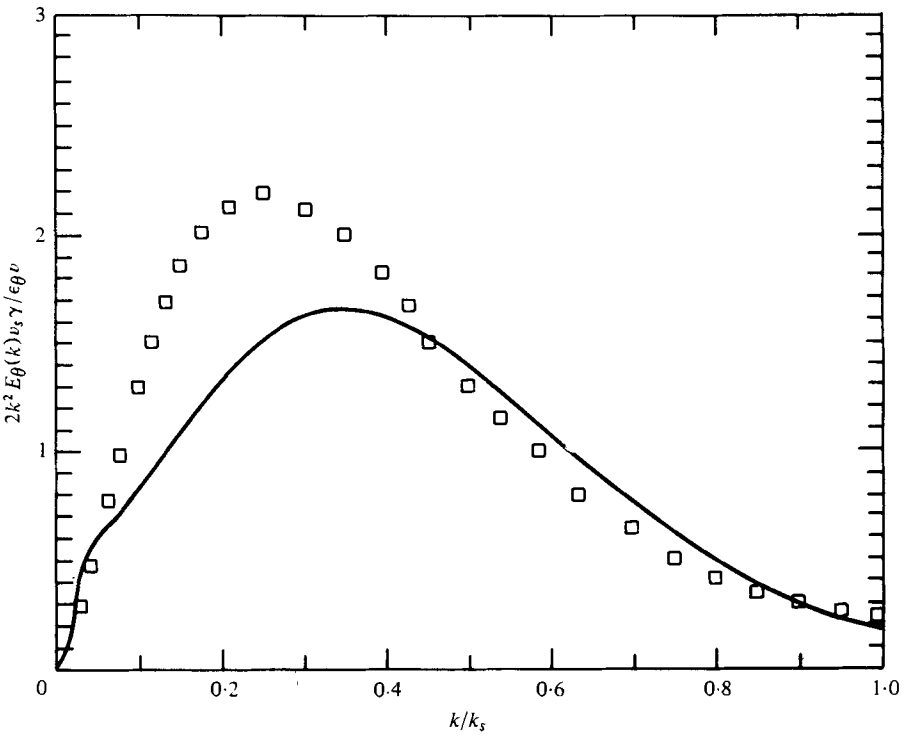

FIGURE 8. Normalized three-dimensional scalar dissipation spectra. ——, our TFM prediction; □, data of Yeh & Van Atta (1973).

over the entire spectrum. In fact, the peak value of the Van Atta & Chen (1969) dissipation spectrum [where their turbulence Reynolds number is almost identical with that of Yeh & Van Atta (1973)] is nearly equal to ours. In addition, we may consider the areas enclosed by the dissipation spectra. With the normalization employed in figures 7 and 8 the areas enclosed by the velocity and scalar dissipation spectra should both be unity. Indeed, we find that the areas enclosed by the TFM spectra (including tail regions not shown on the plots) are nearly identically unity and that the area enclosed by the velocity dissipation spectrum of Yeh & Van Atta (1973) over the reported range, $k/k_s \in (0{\cdot}0, 1{\cdot}0)$, is approximately 0·98. On the other hand, the area enclosed by Yeh & Van Atta's (1973) scalar dissipation spectrum over the reported wavenumber range exceeds unity by about 10 %, and this fact may explain in part the noted difference between the predicted and experimental scalar dissipation spectral peak values.

Finally, we compare in figures (9 and 10) and (11 and 12) longitudinal second-order and third-order correlations, respectively. We define the longitudinal second-order correlations as

$$R(u,u)(d) = \langle u(\mathbf{x})\, u(\mathbf{x}+\mathbf{d})\rangle / \langle u^2(\mathbf{x})\rangle,$$
$$R(\theta,\theta)(d) = \langle \theta(\mathbf{x})\, \theta(\mathbf{x}+\mathbf{d})\rangle / \langle \theta^2(\mathbf{x})\rangle,$$

and we further define the longitudinal third-order correlations as

$$R(uu,u)(d) = \langle u^2(\mathbf{x})\, u(\mathbf{x}+\mathbf{d})\rangle / \langle u^2(\mathbf{x})\rangle^{\frac{3}{2}},$$
$$R(u\theta,\theta)(d) = \langle u(\mathbf{x})\, \theta(\mathbf{x})\, \theta(\mathbf{x}+\mathbf{d})\rangle / \langle u^2(\mathbf{x})\rangle^{\frac{1}{2}} \langle \theta^2(\mathbf{x})\rangle.$$

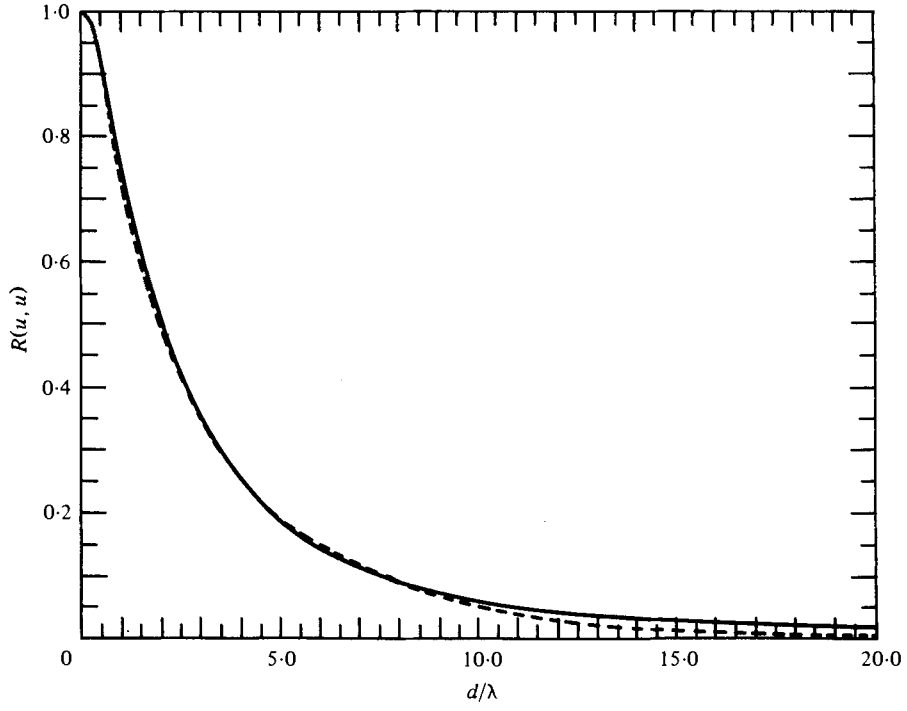

FIGURE 9. Longitudinal second-order velocity correlations. ——, our TFM prediction; – – –, data of Yeh & Van Atta (1973).

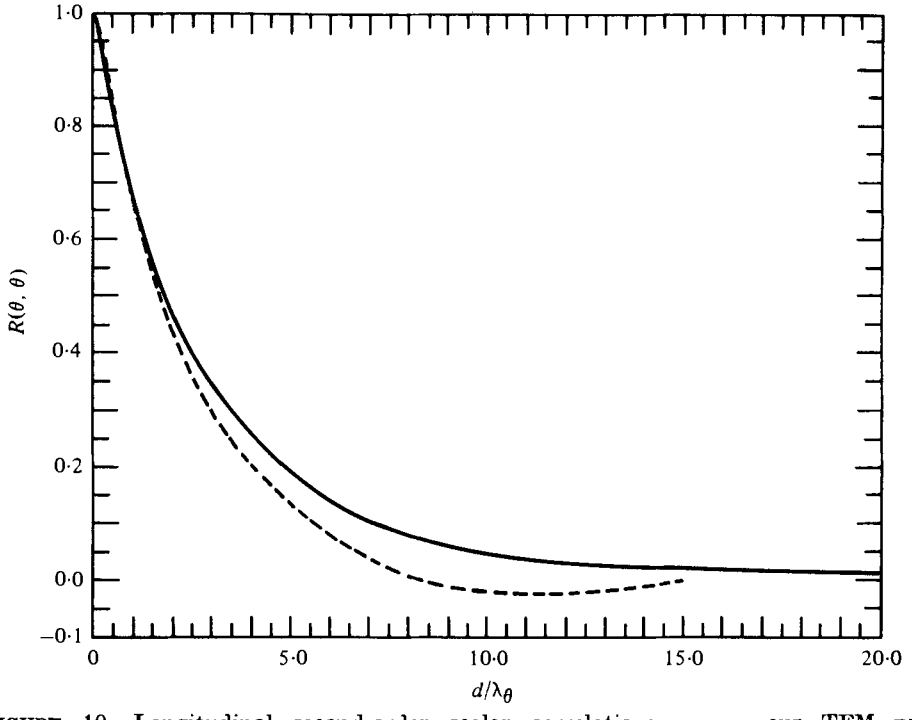

FIGURE 10. Longitudinal second-order scalar correlations. ——, our TFM prediction; – – –, data of Yeh & Van Atta (1973).

For isotropic turbulence all four correlations are functions of only the separation distance magnitude d, $d = (d_i d_i)^{\frac{1}{2}}$. We assume here that the direction of $\mathbf{d}$ points along the direction of the velocity component u. The empirical data are presented in the original paper as functions of a temporal separation variable, whereas we present them as functions of d by making recourse to Taylor's hypothesis. The correlation curves for the simulations are determined with the following formulae which are valid for isotropic turbulence (Monin & Yaglom 1975):

$$R(u,u)(d) = -2/\langle u^2(\mathbf{x})\rangle \int_0^\infty [\cos(kd)/(kd)^2 - \sin(kd)/(kd)^3]\, E(k)\, dk, \tag{3.9}$$

$$R(\theta,\theta)(d) = 2/\langle \theta^2(\mathbf{x})\rangle \int_0^\infty [\sin(kd)/(kd)]\, E_\theta(k)\, dk, \tag{3.10}$$

$$R(uu,u)(d) = -2/\langle u^2(\mathbf{x})\rangle^{\frac{3}{2}} \int_0^\infty [\sin(kd)/(kd)^2 + 3\cos(kd)/(kd)^3 - 3\sin(kd)/(kd)^4]\, T(k)\, dk/k, \tag{3.11}$$

$$R(u\theta,\theta)(d) = 1/\langle u^2(\mathbf{x})\rangle^{\frac{1}{2}} \langle \theta^2(\mathbf{x})\rangle \int_0^\infty [\cos(kd)/(kd) - \sin(kd)/(kd)^2]\, T_\theta(k)\, dk/k. \tag{3.12}$$

We see from the correlation formulae that $R(u,u)$ and $R(\theta,\theta)$ are even functions of the separation d while $R(uu,u)$ and $R(u\theta,\theta)$ are odd functions of d.

Figure 9 shows good agreement between prediction and measurement for the second-order velocity correlation, $R(u,u)(d)$, whereas figure 10 shows moderate agreement for the second-order scalar correlation $R(\theta,\theta)(d)$. Figure 11 gives profiles of $R(u\theta,\theta)$ and $R(\theta,u\theta)$, and moderate agreement between simulation and empirical profiles is evidenced at the smaller values of non-dimensional separation distance. The crossing of the $R(u\theta,\theta)$ and $R(\theta,u\theta)$ data curves at the larger separations is not reproduced by the simulation curves, however. Finally, figure 12 shows only fair agreement between simulation and data profiles of $R(uu,u)$ and $R(u,uu)$. The data profiles are not anti-symmetrical, however, and the $R(uu,u)$ data curve is somewhat better reproduced by simulation than the $R(u,uu)$ curve.

4. Large Reynolds number results

Introduction

We now discuss the TFM for large Reynolds number flows, in which an appreciable inertial range exists. There are two issues here: how well does the TFM work for inertial range wavenumbers, and what is its accuracy in the dissipation range? With regard to the first issue, we shall seek values for (g_v, g_θ) which fit experimental inertial range spectra ($\phi_v(k_1)$ and $\phi_\theta(k_1)$, (2.11) and (2.12)). The correctness of the qualitative aspects of the TFM inertial range is assured by the Lagrangian structure of the theory. We then ask how accurate is the theory for the (universal) dissipation spectra, $k^2\phi_v(k)$ and $k^2\phi_\theta(k)$. The experiments to which we compare theoretical results are the recent observations in the planetary boundary layer reported by Champagne *et al.* (1977). Having thus fixed (g_v, g_θ) for a Prandtl number unity fluid (0·7), and examined the theory's accuracy in the dissipation range, we then examine theoretical predictions for the viscous–convective inertial range at large Prandtl number, and the inertial–diffusive range for very small Prandtl number fluids.

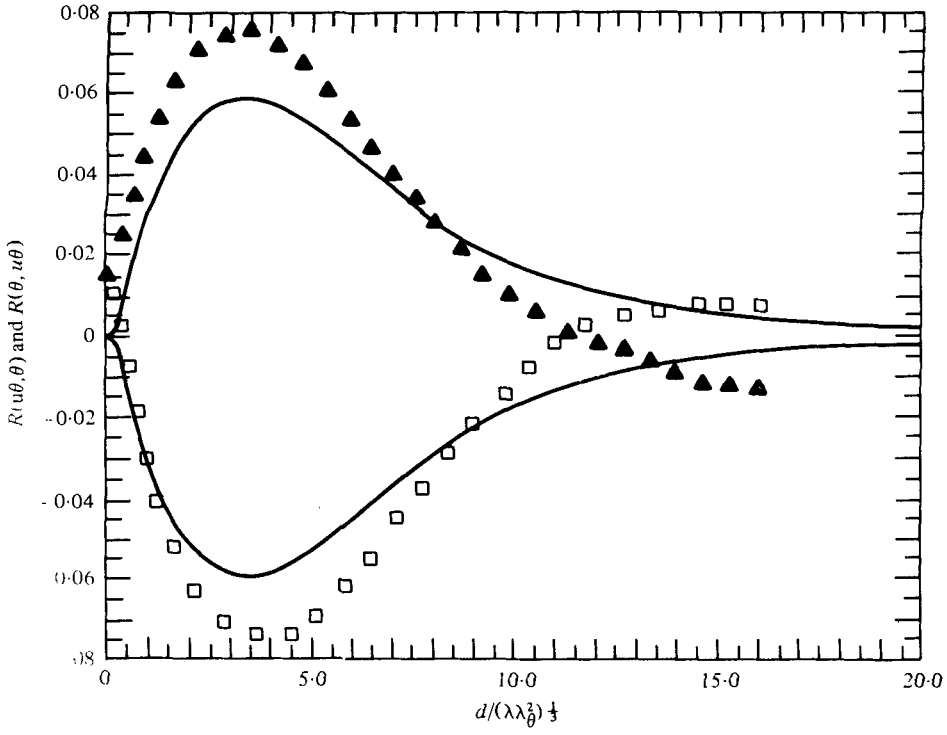

FIGURE 11. Longitudinal third-order mixed velocity-scalar correlations. ——, our TFM predictions; ▲, □, data of Yeh & Van Atta (1973).

Convective inertial range

Calculations of the inertial range coefficients for Prandtl number unity proceed by methods suggested by Kraichnan (1966) and Leith & Kraichnan (1972). We consider stationary turbulence on a trucated wavenumber span (k_0, k_1) maintained by random stirring forces at small k so that both $E(k)$ and $E_\theta(k)$ are proportional to $k^{-\frac{5}{3}}$. We further suppose that the Reynolds (and Péclet) numbers are so large that direct effects of viscosity and conductivity may be entirely ignored. Then if C is the Kolmogorov constant, β_3 the corresponding Oboukhov–Corrsin constant and k_e is an inertial range wavenumber,

$$-1 = C^{\frac{3}{2}} \int_{k_0}^{k_e} dk\, T_v(k), \tag{4.1}$$

$$-1 = \beta_3 C^{\frac{1}{2}} \int_{k_0}^{k_e} dk\, T_\theta(k). \tag{4.2}$$

Here, T_v is $(4\pi k^2)$ times the right-hand side of (2.18) if $U(k) = k^{-\frac{11}{3}}$ is used in its evaluation, and if further $D(k, p, q)$ is evaluated from (2.20) with $dD(k, p, q)/dt = 0$, and the above $U(k)$ spectrum is used to specify $\eta^s(k)$ and $\eta^c(k)$. Similarly, $T_\theta(k)$ is $(4\pi k^2)$ times the right-hand side of (2.27) if $U(k)$ and $\theta(k)$ are both $k^{-\frac{11}{3}}$, and if $D^\theta(k, p, q)$ is specified in analogy with $D(k, p, q)$. This prescription calls for solving a pair of equations for η^s and η^c for $U(k) = k^{-\frac{11}{3}}$. Physically the calculation is based on the observation that if a $k^{-\frac{5}{3}}$ spectrum is maintained by random stirring forces on a truncated wavenumber span (k_0, k_1) then these forces will be non-vanishing only near

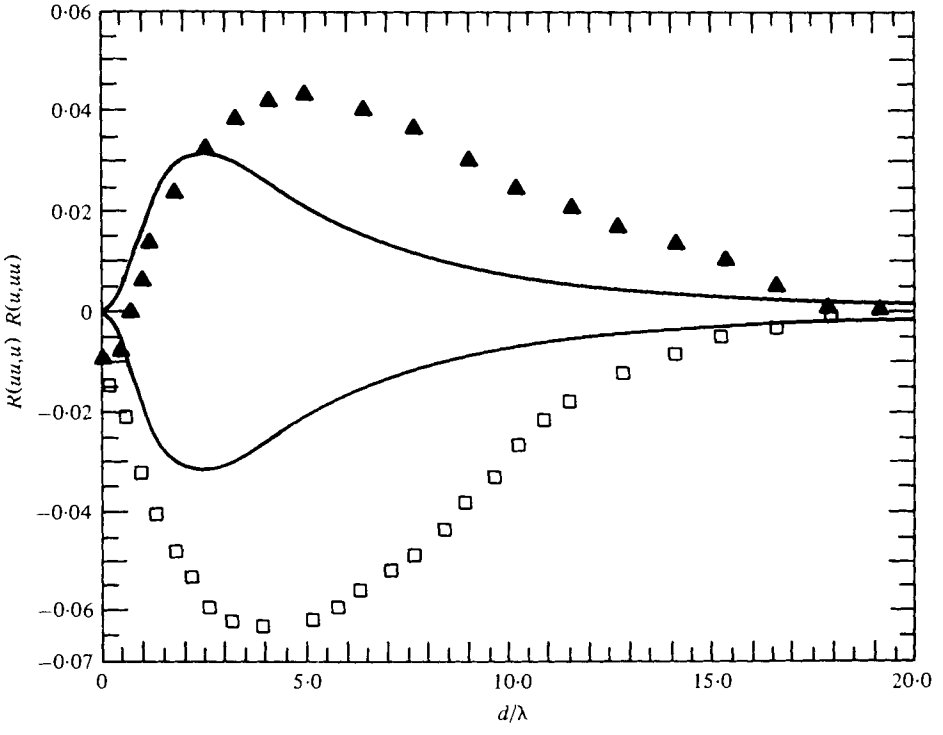

FIGURE 12. Longitudinal third-order velocity correlations. ——, our TFM predictions; ▲, □, data of Yeh & Van Atta (1973).

k_0 and k_1. If $k_0 \ll k_e \ll k_1$, $T(k_e) \cong 0$, and C may be evaluated by equating the flux of energy out of the small wavenumber region ($k \leqq k_e$) to dissipation above k_1. The present calculations employ $k_0 = 0{\cdot}1$, $k_1 = 100$, which is the identical wavenumber span used by Leith & Kraichnan (1972) in their determination of the Kolmogorov constant, C (4.1). Their calculation gave

$$C = 1{\cdot}348 g_v^{\frac{2}{3}}, \tag{4.3}$$

and, as noted earlier, the choice $g_v = 1{\cdot}5$ implies $C = 1{\cdot}78$, in good agreement with the ALH (Kraichnan 1966), and the large Reynolds number data of Grant, Stewart & Moilliet (1962). We retain this choice of g_v and require a value of g_θ which gives

$$\beta_3 = 0{\cdot}40 \times \tfrac{5}{3}, \tag{4.4}$$

a value in agreement with observations of Champagne *et al.* (1977) and others. Table 1 shows $\beta_3(g_v = 1{\cdot}5, g_\theta)$ for a range of g_θ. We note the relative insensitivity of β_3 to g_θ, and observe that $g_\theta^2 \cong 0{\cdot}25$ is in good agreement with the data.

We next examine the predictions of the TFM for the large Reynolds number flows, using the above values for g_v and g_θ. Comparisons are for the Kolmogorov's normalized dissipation spectra,

$$2(k/k_s)^2 \phi_v(k)/(v_s^2 k_s), \tag{4.5}$$

and

$$k^2 \phi_\theta(k)\, v_s/N. \tag{4.6}$$

In (4.6), N is the dissipation of θ. The normalization of these spectra is such that the integral of (4.5) over all k/k_s is $\frac{1}{6}$ and the integral of (4.6) is $Pr/3$, where Pr is the

g_θ^2	0·20	0·25	0·30	0·35
β_s	0·63	0·67	0·70	0·73

TABLE 1

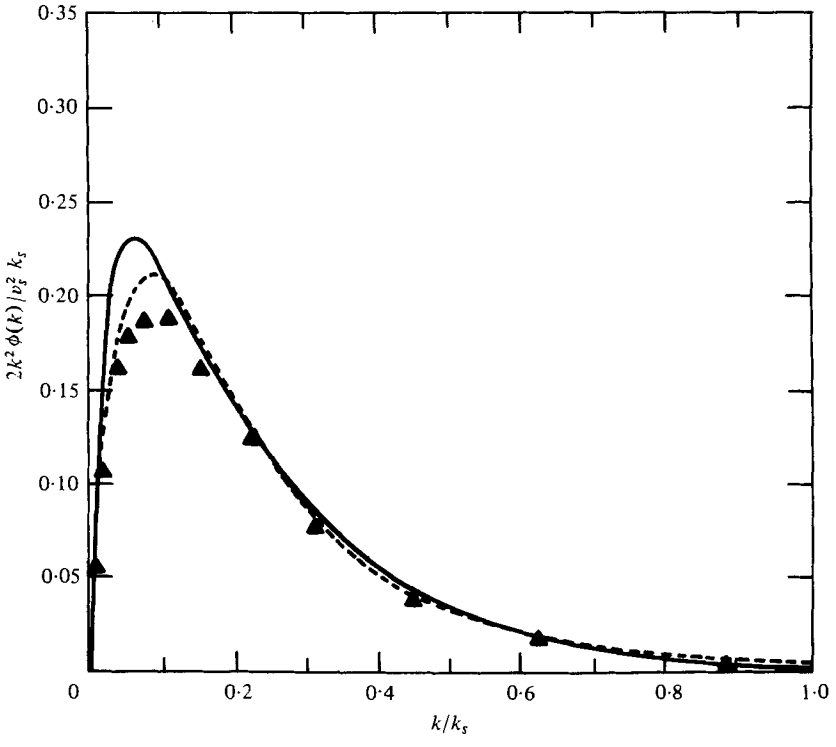

FIGURE 13. TFM normalized one-dimensional energy dissipation spectra (——) compared to smoothed data of Champagne *et al.* (1977) (– – – –), and to the data of Williams (1974) (▲).

Prandtl number, ν/γ. Figure 13 shows the comparison of computed spectra to the data of Champagne *et al.* (1977). The computed spectra had initial values specified by (3.1), and R_λ during the self-similar decay portion of the run was $\simeq 250$. Our previous experience with decay problems indicated that the dissipation spectrum reaches its asymptotic profiles at $R_\lambda \gtrsim 100$. The comparison with the velocity data is good and in substantial agreement with previous calculations of Herring & Kraichnan (1972). The agreement with temperature data is somewhat poorer, but still such as to reproduce the major features of the observational spectrum. The agreement at large $k/k_s (\gtrsim 0{\cdot}9)$ is poorest, but Champagne *et al.* remark that data in this region are contaminated by instrumental noise, so that the actual spectrum at large k/k_s should be smaller than the displayed data by a few per cent. Just how to interpret the degree of agreement of a particular theory and observations is a difficult question. As remarked earlier, spectra (4.5) and (4.6) are normalized, so that the area under the curves is fixed.

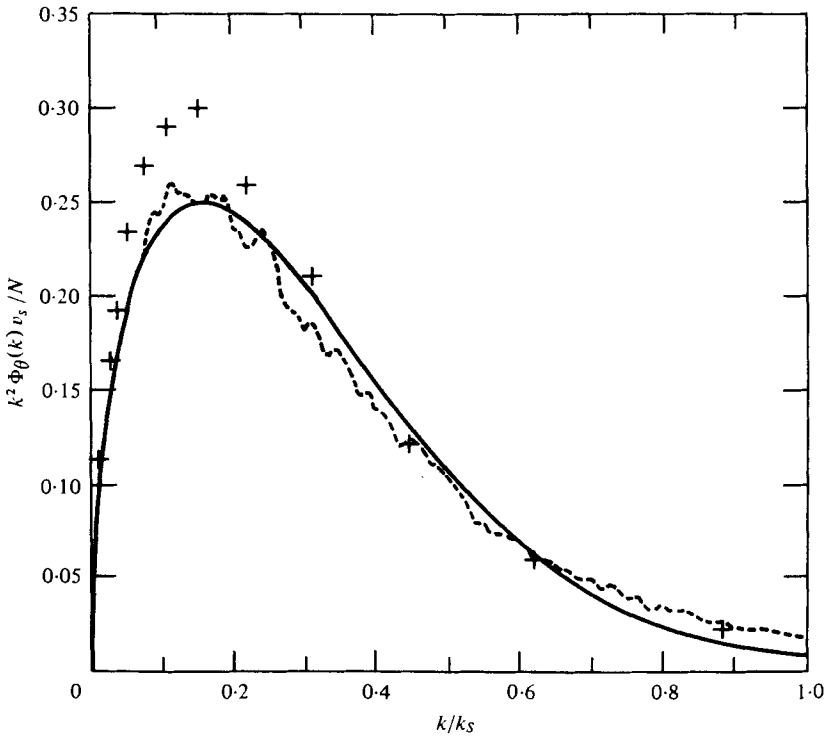

FIGURE 14. TFM normalized one-dimensional scalar dissipation spectrum(——) as compared with the data of Champagne *et al.* (1977) (– – –), and to the data of Williams (1974) (+).

Viscous convective range

We now discuss the TFM's predictions for very large Prandtl number fluids. In this case, the θ-inertial range extends far beyond the velocity dissipation range, k_s, and we may evaluate the θ-transfer function [which is $4\pi k^2$ times the right-hand side of (2.27)] as if $U(q)$ were composed of a random straining field at near-zero wavenumber. The procedure needed is to expand $U(q)$ about $q = 0$, and retain the first non-vanishing terms (Kraichnan 1968). There results for the right-hand side of (2.27)

$$\frac{1}{15}\int_0^\infty p^2E(p)\,dp[k^2\partial^2\Theta(k)/\partial k^2 + 4k\partial\Theta/\partial k]/[\eta^s(p) + 2g_\theta^2\eta^c(k)], \tag{4.7}$$

which yields Batchelor's viscous–convective subrange,

$$\phi_\theta(k) = N(\nu/\epsilon)^{\frac{1}{2}}C_B\,k^{-1}, \tag{4.8}$$

where

$$C_B = \tfrac{5}{2}(\epsilon/\nu)^{-\frac{1}{2}}\Big/\int_0^\infty dp\,p^2E(p)/[\eta^s(p) + 2g_\theta^2\eta^c(k)], \tag{4.9}$$

During the self-similar portion of the decay, our calculation yields

$$C_B = 1{\cdot}68, \tag{4.10}$$

for large $R_\lambda(\approx 250)$. This value is slightly lower than Gibson's (1968) bound, $\sqrt{3}$, but nonetheless in fair agreement with the data of Gibson (1962) and Clay (1973), who

obtained $C_B \simeq 2{\cdot}0$. If $g_\theta = 0$, which seems appropriate if $g_\theta \eta^c$ is interpreted strictly as a Lagrangian-scalar relaxation time, $C_B = 0{\cdot}68$ results. This unreasonably small value is close to Kraichnan's ALHDI estimate $C_B \lesssim 0{\cdot}9$.

Finally, for completeness, we should note that for $k \gtrsim (\epsilon/\nu\gamma^2)^{\frac{1}{4}} \equiv k_\theta$, (4.8) must be replaced by a conductive dissipation range, in which $2\gamma k^2\theta(k)$ is equal to (4.7). The theory predicts

$$\phi_\theta(k) = NC_B(k^{-1} + 2^{\frac{1}{2}}k_\theta^{-1}) \exp(-2^{\frac{1}{2}}k/k_\theta), \tag{4.11}$$

which differs from Batchelor's $k^{-1}\exp(-(k/k_\theta)^2)$ prediction but is identical to Kraichnan's analysis of a scalar convected by a stochastic velocity field (Kraichnan 1968).

Conductive inertial range

By inspection, the TFM scalar equation reduces to the (Markovian) quasi-normal approximation for very low Prandtl numbers. Thus, we retrieve in this limit the results of Batchelor, Howels & Townsend (1959).

5. Evaluation of second-order closure quantities

Introduction

In this section we evaluate normalized decay rates for the scalar and velocity dissipation rates from self-similar TFM predictions of decaying, isotropic scalar turbulence. We define these normalized decay rates as:

$$\psi \equiv -\dot{\epsilon}\overline{q^2}/\epsilon^2, \quad \psi_\theta \equiv -\dot{\epsilon}_\theta\overline{\theta^2}/\epsilon_\theta^2, \tag{5.1}$$

where the single-point moments ($\overline{q^2}$, $\overline{\theta^2}$, ϵ and ϵ_θ defined previously) are functions of time only for isotropic scalar turbulence. These normalized decay rates may be viewed as the second-order closure parameters for the second-moment equations which describe isotropic scalar turbulence. We record these equations here:

$$\dot{\overline{q^2}} = -2\epsilon, \quad \dot{\overline{\theta^2}} = -2\epsilon_\theta, \tag{5.2}$$

$$\dot{\epsilon} = -\psi\epsilon^2/q^2, \quad \dot{\epsilon}_\theta = -\psi_\theta\epsilon^2\theta/\overline{\theta^2}.$$

We observe that if ψ and ψ_θ are parameterized in terms of $\overline{q^2}$, $\overline{\theta^2}$, ϵ and ϵ_θ (as is done in second-order modelling), then the system (5.2) forms a closed, predictive set. We shall, in addition, evaluate the ratio of the velocity time scale $\overline{q^2}/\epsilon$, to the scalar time scale $\overline{\theta^2}/\epsilon_\theta$, which we denote as $r \equiv (\overline{q^2}/\epsilon)/(\overline{\theta^2}/\epsilon_\theta) \equiv$ the time scale ratio. This quantity has been found to be useful in the construction of a second-order closure model for homogeneous scalar turbulence (Newman, Launder & Lumley 1979). We may view the scales $\overline{q^2}/\epsilon$ and $\overline{\theta^2}/\epsilon_\theta$ as the time scales for significant changes in the large-scale (energy containing) velocity and scalar eddies, respectively. We shall compare our prediction results for ψ, ψ_θ and r with results obtained from heated grid experiments.

Simulation results and comparison with experiments

We have performed a number of TFM simulations of scalar decay in isotropic turbulence for various Reynolds numbers, Prandtl numbers and initial spectral shapes (which evolve into self-preserving forms). The Reynolds number range spanned in the simulations is $R_\lambda = 3{\cdot}2$ to $R_\lambda = 62{\cdot}5$ while the Prandtl number range is 0·01 to 10. In addition, we have also varied the values of g_v and g_θ. We present here the results for

Run	Spectrum	Initial peak wave-number	R_λ at t_{final}	Prandtl number	g	t_{final}	P_λ at t_{final}
1	E	3·3	61·5	1·0	1·0	0·8	56·8
	E_θ	6·6					
2	E	9·1	24·1	1·0	1·0	3·0	25·4
	E_θ	18·2					
3	E	18·2	22·0	1·0	1·0	3·0	24·3
	E_θ	9·1					
4	E	9·1	52·8	0·1	1·5	0·5	17·7
	E_θ	9·1					
5	E	9·1	36·9	4·0	1·5	0·6	74·9
	E_θ	9·1					

TABLE 2

ψ, ψ_θ and r from five of the simulations; the initial conditions and parameter values for the five simulations (which are denoted as runs 1–5) are given above in table 2. In the simulations presented here, we have employed $g_v = g_\theta = g$ with g varying from 1·0 to 1·5, and we have utilized the spectral form given in (3.1) to initialize $E(k)$ and $E_\theta(k)$. On the other hand, the results presented here are representative of those for our entire set of simulations (including those in which $g_v \neq g_\theta$), because the asymptotic behaviours of ψ, ψ_θ and r are very similar for the entire prediction set. Before considering the simulation results, we first describe the general evolutionary behaviours exhibited in our predicted energy spectra.

Our simulations depict the evolution toward self-preservation of isotropic scalar and velocity fields which are initialized by prescribed profiles for $E(k)$ and $E_\theta(k)$ and by zero initial spectral transfer. The initial energy spectra are distinguishable in terms of the positions of their peaks, and from table 2 we observe that $E(k)$ and $E_\theta(k)$ initially peak at different wavenumbers in some of the runs considered here. For the 'well behaved' energy spectra employed in our simulations, we may view the relation between the wavenumbers of the peaks in $E(k)$ and $E_\theta(k)$ as depicting the inverse relation between the sizes of the large-scale (energy containing) velocity and scalar eddies. On the other hand, the evolution of the velocity and scalar spectra exhibit (qualitatively) universal characters in all of our simulations after self-preservation is approximately achieved. In the self-preserving mode, all of our simulations predict that both $E(k)$ and $E_\theta(k)$ peak at successively lower wavenumbers as time increases, and, further, in all of the simulations the $E_\theta(k)$ spectra peak at somewhat lower wavenumbers than the corresponding $E(k)$ spectra. We note that both of these characteristics are exhibited in the heated grid turbulence data of Yeh & Van Atta (1973). In real turbulence, the former characteristic reflects the fact that, although eddy energy is cascaded toward the higher wavenumbers, the smaller eddies decay more rapidly than the larger ones. We now consider the second-order parameterizations and the time scale ratio.

In figure 15 we present the results for r from runs 1–5 while in figures 16 and 17 we give the results for ψ and ψ_θ from these runs. In these figures the quantities are given as functions of the dimensional simulation time, t. The striking feature of these plots is that the curves for the time scale ratio appear to be asymptoting to values in the neighbourhood of $r \simeq 1$, while the curves for both ψ and ψ_θ appear to be asymptoting to

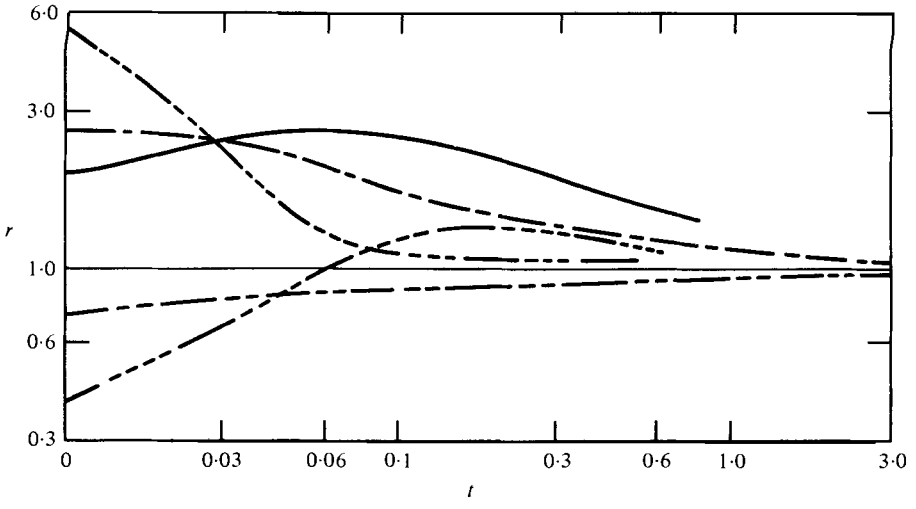

FIGURE 15. Time scale ratio. ——, run 1; – – –, run 2; – – – –, run 3; – – – – –, run 4; – – – – – –, run 5.

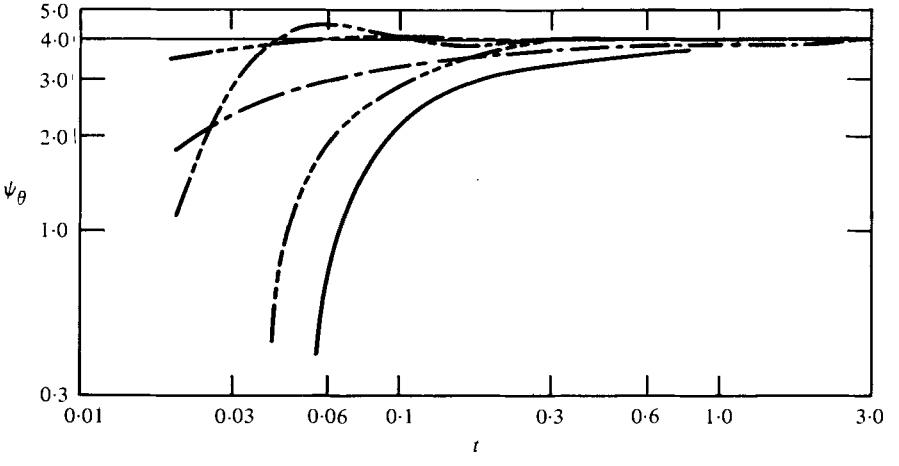

FIGURE 16. Second-order parameterization for the velocity dissipation equation. ——, run 1; – – –, run 2; – – – –, run 3; – – – – –, run 4; – – – – – –, run 5.

values in the neighbourhood of ψ, $\psi_\theta \simeq 4$. Further, these asymptotic behaviours seem independent of the level of R_λ and of the value of the Prandtl number over the ranges of these two quantities spanned by the simulations. In fact, we find similar asymptotic results for ψ, ψ_θ and r from all of our simulations. Changes in the levels of R_λ and P_λ appear only to influence the rate at which predictions evolve to self preservation. In addition, in all of our simulations, the decays of $\overline{q^2}$ and $\overline{\theta^2}$ asymptote nearly to power law decays where the decay exponents are nearly unity for both quantities. These decay trends for $\overline{q^2}$ and $\overline{\theta^2}$ are consistent with the asymptotic approach of ψ and ψ_θ toward values in the neighbourhood of 4. Indeed, ψ and ψ_θ reduce to the following simple forms for the case of power law decay for $\overline{q^2}(t)$ and $\overline{\theta^2}(t)$:

$$\psi = -2(1+1/n_v), \quad \psi_\theta = -2(1+1/n_\theta), \tag{5.3}$$

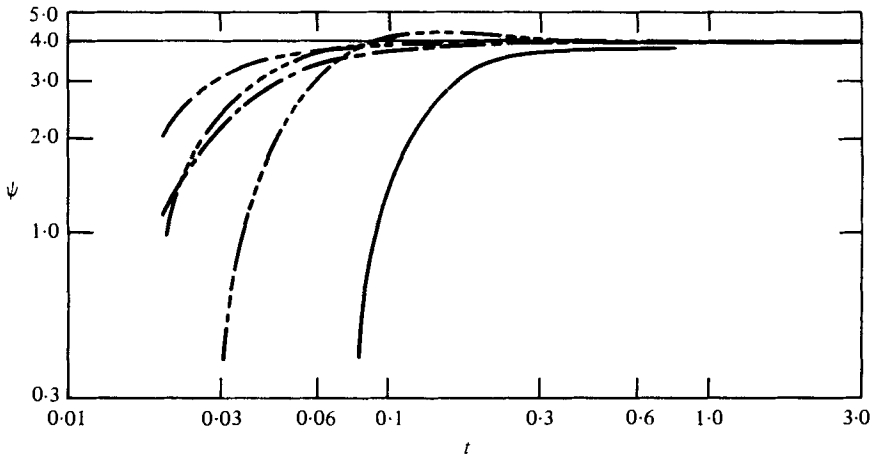

FIGURE 17. Second-order parameterization for the temperature dissipation equation. ——, run 1; — — —, run 2; – – – –, run 3; ——– ——, run 4; ——– – ——, run 5.

where n_v and n_θ are the $\overline{q^2}$ and $\overline{\theta^2}$ power law exponents, respectively, and where these forms are valid independent of possible non-zero virtual origins for $\overline{q^2}$ and $\overline{\theta^2}$; we obtain ψ, $\psi_\theta = 4{\cdot}0$ upon setting n_v, $n_\theta = 1{\cdot}0$ in (5.3).

The apparent insensitivity of the asymptotic values of r, ψ and ψ_θ to changes in R_λ and P_λ implies that these quantities are not influenced by changes in the levels of the scalar and mechanical molecular diffusivities in the TFM. This phenomenon, if observed, would probably be exhibited in real isotropic turbulence only for cases of moderate to large Reynolds and Péclet numbers [consistent with the ideas of non-linear (inviscid) velocity and scalar energy cascades]. Partial support of this premise may be inferred from the modelling work of Lumley & Newman (1977). These authors formulate a second-order closure model for isothermal, anisotropic, homogeneous turbulence using the invariant modelling techniques developed by Lumley (1970). The forms for their parameterized closures are determined in part from requirements of realizability (after Schumann 1977), in part from existing homogeneous turbulence decay data, and in part from consideration of various analytical results for limiting states of homogeneous turbulence. If we specialize their representation for ψ to the case of isotropic turbulence we obtain

$$\psi = \tfrac{14}{5} + 0{\cdot}980 \exp\left[-2{\cdot}83/R_l^{\frac{1}{2}}\right], \tag{5.4}$$

where $R_l (\equiv (\overline{q^2})^2/9\epsilon\nu)$ is the turbulence Reynolds number based on the integral length scale. The form (5.4) indicates that ψ changes by about only 6 % over the range $R_l^{\frac{1}{2}} \simeq 10$ to $R_l^{\frac{1}{2}} \to \infty$, although we note that the asymptotic value, $\psi = 3{\cdot}78$ as $R_l^{\frac{1}{2}} \to \infty$, is extrapolated from existing grid turbulence data which span $R_l^{\frac{1}{2}}$ values only up to $R_l^{\frac{1}{2}} \simeq 40$. Consequently, our predicted value for self-similar decay with the TFM, $\psi = 4{\cdot}0$, agrees to within 11 % with the levels of ψ appropriate for grid turbulence over the observed range for $R_l^{\frac{1}{2}} \geqslant 10$. We now consider the levels of r found in heated turbulence data.

Warhaft & Lumley (1978) review the existing empirical data concerning (isotropic) heated grid turbulence and present new data from their experimental studies of

heated grid turbulence. The scalar contaminant, temperature, behaved passively in most of the flows examined. The levels of ψ in the data are adequately represented by the second-order expression (5.4) and hence in reasonable agreement with the self-similar TFM value. The scalar and velocity variance decay data for all of the heated grid flows are adequately represented by power law forms so that the time scale ratio equals the ratio of the exponents, $r = n_\theta/n_v$. By virtue of the power law representations we see that the level of r [and hence the levels of ψ and ψ_θ, from (5.3)] is invariant with respect to streamwise position in any flow; however, the level of r varies from approximately 0·6 to 2·4 among the different data sets. In addition, the measurements of Warhaft & Lumley (1978) suggest that the level of r in thermal grid turbulence may be a unique function of the ratio k_v/k_θ where k_v and k_θ are the wavenumbers corresponding to the peaks of the three-dimensional velocity and scalar energy spectra. Their measurements indicate that the ratio k_v/k_θ remains approximately uniform independent of streamwise position in each of their flows [although both k_v and k_θ decrease with downstream position consistent with the results of Yeh & Van Atta (1973)], and Warhaft & Lumley (1978) propose that the invariance of the level of r in a decaying, thermal grid turbulence flow may derive from the observed invariance of the ratio k_v/k_θ. Further, the data of Warhaft & Lumley (1978) indicate that the level of $r = 1{\cdot}0$ in scalar grid turbulence occurs when $E(k)$ peaks at a wavenumber approximately 25 % higher than $E_\theta(k)$. This result concurs moderately well with the results of Yeh & Van Atta (1973), and this difference in the $E(k)$ and $E_\theta(k)$ peak wavenumbers is fairly well reproduced in our TFM predictions which give $r = 1$. We note that the normalized energy and dissipation spectra obtained by Warhaft & Lumley (1978) (for the case of $r = 1$) at levels of R_λ and P_λ comparable to those of Yeh & Van Atta (1973) are in fairly good agreement with the corresponding normalized spectra obtained by Yeh & Van Atta (1973). Warhaft & Lumley (1978) did not measure transfer spectra or triple correlations, however.

We observe that the grid flows with values of $r \neq 1$ differ from our TFM simulations with regard to the behaviour of the time scale ratio (and hence of ψ_θ). The empirical data indicate that r is invariant with respect to streamwise position over distances corresponding to evolutionary periods up to one turbulence decay time (where we define the turbulence decay time, τ, by $d\tau = \epsilon/\overline{q^2}\,dt$); whereas in the simulations r asymptotes from its initial level to the value $r \simeq 1$ within this evolutionary period. This discrepancy may derive in part from the aforementioned difficulty (caused by differences in initial conditions) in assessing to what extent the evolutionary periods of the TFM simulations match those of the grid flows. It is possible that the behaviour of r (and ψ_θ) exhibited in the grid flow data would be better predicted if the theory prescriptions could be altered so that the initial spectra profiles more nearly reproduced the initial empirical spectra. On the other hand, it is interesting to interpret the results in the light of a possible 'equilibrium' decay regime for isotropic scalar turbulence (after Newman *et al.* 1979).

As noted above, the self-similar TFM result of $\psi \simeq 4$ agrees quite well with existing data for $R_l^{\frac{1}{2}} \geqslant 10$, and this suggests that the self-similar TFM value of $r \simeq 1$ ($\psi_\theta \simeq 4$) may be the appropriate asymptotic (equilibrium) value for decaying isotropic scalar turbulence for moderate and large Reynolds and Péclet numbers. The value of $r \simeq 1$ for a decaying 'equilibrium' flow (which is not influenced by initial or boundary conditions) is appealing from the physical viewpoint. That is, it seems plausible (Newman

et al. 1979) that cumulative distortions of the scalar field by the velocity field in decaying isotropic scalar turbulence would alter the $E_\theta(k)$ spectrum to a distribution consistent with equilibrium decay with the $E(k)$ spectrum; the large eddy (energy containing) length scales of the scalar and velocity field would presumably be comparable in this equilibrium regime (i.e. $k_v/k_\theta \simeq 1$) and the time scale ratio approximately unity. Our TFM simulation results are consistent with this picture of asymptotic equilibrium decay, but the heated grid data evidencing values of $r \neq 1$ apparently are not. On the other hand, it is possible that the grid flows were not of sufficient streamwise extent for equilibrium decay to be established (i.e. that the behaviour of r was everywhere influenced by initial conditions behind grids); although one would expect some tendency for evolution toward equilibrium decay to have been evidenced in at least the longest flows examined (Newman *et al.* 1979). In addition, we note that the Reynolds numbers of the heated grid flows are fairly low [with the exception of the flows of Lin & Lin (1973), which have quite short streamwise extents]. Lumley & Newman (1977) have shown that the rate of return to isotropy of the velocity field in homogeneous turbulence without mean shear increases with increasing Reynolds number. It is possible that the behaviour of r in heated grid flows may also vary with Reynolds number so that an equilibrium level of $r \simeq 1$ might be attained fairly rapidly (consistent with the TFM simulations) in a grid flow with large Reynolds number. Further grid turbulence experiments might shed light on this equilibrium decay issue.

6. Summary and discussion

In this investigation, the test field model (Kraichnan 1971) was applied to the study of the decay of isotropic, passive-scalar turbulence. TFM simulation results at large Reynolds/Péclet numbers for scalar and velocity dissipation spectra were shown to be in excellent agreement with the atmospheric data of Champagne *et al.* (1977), after the intrinsic scale constants in the TFM were adjusted to provide for agreement between predicted and empirical one-dimensional energy spectra in the inertial wavenumber range. Although the theory does have an adjustable constant, it does yield the correct Batchelor number at high Prandtl number, if the constant is chosen to give the correct Oboukhov–Corrsin constant. Further, predicted self-similar velocity and scalar energy, dissipation and transfer spectra and second- and third-order velocity, scalar and velocity–scalar correlations at moderate Reynolds and Péclet numbers were shown to provide moderate agreement with the heated grid turbulence data of Yeh & Van Atta (1973) (which exhibited near-unity levels of the ratio of velocity to scalar time scales, r). In addition, self-similar decay results from the simulations exhibited an asymptotic approach to values approximately unity for r and to values about equal to 4·0 for the normalized decay rates of the velocity and scalar dissipation rates, ψ and ψ_θ, respectively.

The predicted level for ψ was shown to agree quite well with levels of ψ observed in grid turbulence data over the experimental Reynolds number range, $R_l^{\frac{1}{2}} \geqslant 10$. On the other hand, the predicted asymptotic approach to $\psi_\theta = 4{\cdot}0$, $r = 1$ within one turbulence decay time was noted to be at variance with existing heated grid turbulence data (in which $r \neq 1$) in which ψ_θ and r remain invariant at their initial values over comparable evolutionary periods. These disparities were discussed in the context of

'equilibrium' decay of concomitant, isotropic scalar and velocity fields (after Newman *et al.* 1979), and a consistent picture was discussed in which the predicted results for ψ_θ and r were viewed as equilibrium decay values, appropriate for moderate and large Reynolds and Péclet numbers, which might be observed asymptotically in heated grid turbulence flows. It was suggested that a further study with theory prescriptions altered so that initial spectral forms concur more closely with those observed in heated grid flows might yield predictions which better reproduce the ψ_θ and r behaviours observed in the data. In addition, we discuss briefly here two alternative approaches which might influence agreement between simulations and heated grid data.

As noted, our TFM velocity and scalar spectra and correlation profiles agree moderately well with the empirical profiles of Yeh & Van Atta (1973) at moderate Reynolds and Péclet numbers. On the other hand, these moderate Reynolds number simulations were performed with the values of the intrinsic scale factors (g_v and g_θ) appropriate for large Reynolds number (near unity Prandtl number) flows. As discussed previously, these factors serve to scale the time scales for build-up of the scalar and velocity triple moments. It is possible that the triple moment time scales in real scalar turbulence are Reynolds number dependent, and thus that good agreement between self-similar TFM predictions and empirical data over a wide range of Reynolds number might be achieved by specifying suitable Reynolds number variations for g_v and g_θ. (A Prandtl number dependence may also be appropriate.) However, preliminary investigations of this possibility by comparing simulations with the Yeh & Van Atta (1973) grid data has not proved unambiguous. We performed two TFM simulations of the Yeh & Van Atta (1973) flow employing $g_\theta = g_v = g$ with the values $g = 1{\cdot}0$ and $g = 1{\cdot}5$. Our results show that the larger value of g provides for better agreement with the data for the energy and dissipation spectra. On the other hand, the smaller value yields better agreement between prediction and data for the velocity and velocity–scalar triple correlations, and the smaller value creates larger negative peak values in the $T(k)$ and $T_\theta(k)$ spectra (consistent with increased transfer efficiency as noted in Herring & Kraichnan 1972) which may better correspond to the transfer in low Reynolds number flows (although the noted difficulties in measuring the transfer spectra preclude definitive evaluation of this latter possibility). In the light of these results we chose to employ the established large Reynolds number values for g_v and g_θ for the simulation of the Yeh & Van Atta (1973) flow presented in this paper. Further model comparisons with new data and with new direct numerical simulation results might provide for evaluation of a possible Reynolds number dependence for g_v and g_θ.

A second alternative (after Lesieur & Schertzer 1977) to the approach followed in this work concerns alteration of the forms of the $E(k)$ and $E_\theta(k)$ spectra utilized to initialize the TFM simulations. Lesieur & Schertzer (1977) present results of their theoretical study of decaying, isothermal isotropic turbulence in which they investigate the influence of the form of the initial energy spectrum upon the subsequent temporal evolution of the velocity decay. Lesieur & Schertzer (1977) employed an eddy-damped quasi-Gaussian model which should provide simulations in qualitative agreement with velocity TFM simulations. These authors report that power law decays for $\overline{q^2}$ with unity exponent values are obtained from simulations with initial $E(k)$ spectra which are proportional to k at small k, and their results indicate that

the associated dissipation spectra achieve self-preservation. On the other hand, these investigators report that power law decays for $\overline{q^2}$ with values of the exponents greater than unity (they obtained exponent values in the range 1·3–1·44) are obtained from initial $E(k)$ spectra which tend as k^s ($s \neq 1$) at small k, and for these cases their results show that the associated dissipation spectra have non-self-preserving regions, apparently at variance with the self-preserving nature of grid turbulence dissipation spectra.

The results of Lesieur & Schertzer (1977) suggest that a similar study of the scalar decay problem might prove interesting. That is, it is possible that asymptotic levels of $r \neq 1$ and $\psi_\theta \neq 4{\cdot}0$ might be evidenced in TFM simulations in which the initial $E(k)$ and $E_\theta(k)$ spectra tend as k^s ($s \neq 1$) at small k. The scalar dissipation spectra in such simulations, however, might well also exhibit non-self-preservation in contradistinction to heated grid data. Consequently, the behaviours of r and ψ_θ exhibited in the heated grid data for the cases with $r \neq 1$ might be better reproduced, but at the expense of unfaithful simulation of the dissipation. In addition, we note that absence of self-preservation in simulation results engenders difficulties in comparing prediction with experiment; because, in the absence of a self-similar mode, one should match evolution times between simulation and experiment in order to effect comparison, and this matching is not straightforward. In the work presented in this paper we have employed solely the initial spectral form (3.1) (which tends as k at small k) which yields self-preserving spectra in order to facilitate comparison between prediction and data. However, we note that a future study of the scalar decay problem with different initial spectral forms (after Lesieur & Schertzer 1977) might provide input regarding the question of evolution toward equilibrium decay in isotropic scalar turbulence discussed in the previous section.

The National Center for Atmospheric Research is sponsored by the National Science Foundation.

Appendix

We develop here a test field model for an isotropic scalar field in isotropic turbulence from a Langevin model representation for the scalar equation of motion. The direct interaction approximation (DIA) serves as a reference closure for our Langevin model. Our development parallels that of Kraichnan (1971), and details omitted here may be gleaned from his paper.

The forced equation of motion for a passive scalar contaminant may be written in Fourier space, using the transforms and symbols defined in § 2, as

$$\left(\frac{\partial}{\partial t}+\gamma k^2\right)\theta(\mathbf{k},t)+i\sum_{\mathbf{k}=\mathbf{p}+\mathbf{q}}^{\Delta} k_m v_m(\mathbf{q},t)\,\theta(\mathbf{p},t)=f(\mathbf{k},t), \tag{A 1}$$

where $f(\mathbf{k}, t)$ is a stochastic driving force. The convolution sum,

$$\sum_{\mathbf{k}=\mathbf{p}+\mathbf{q}}^{\Delta},$$

spans all allowed $(\mathbf{p}, \mathbf{q})$ such that $(\mathbf{k}, \mathbf{p}, \mathbf{q})$ form a triangle $(\mathbf{k} = \mathbf{p}+\mathbf{q})$.

To obtain the DIA equations for the scalar field we first form the equations for the ensemble-averaged response Green's function and the scalar covariance [which are obtained from (A 1)] and then apply the DIA algorithm (Kraichnan 1959) to these equations. With these manipulations we obtain the scalar DIA:

$$\left(\frac{\partial}{\partial t}+\gamma k^2\right)G(k,t,t')+\int_{t'}^{t}\hat{\eta}(k,t,s)\,G(k,s,t')\,ds=0 \quad (t>t'),$$

with
$$G(k,t',t')=1, \quad G(k,t,t')=0 \quad (t<t'),$$
$$G(k,t,t')\equiv\langle G(\mathbf{k},t,t')\rangle, \tag{A 2}$$

$$\left(\frac{\partial}{\partial t}+\gamma k^2\right)\Theta(k,t,t')+\int_{-\infty}^{t}\hat{\eta}(k,t,s)\,\Theta(k,s,t')\,ds=\int_{-\infty}^{t}\langle f(\mathbf{k},t)f^*(\mathbf{k},s)\rangle\,G(k,t',s)\,ds$$
$$+\pi k\int_{-\infty}^{t'}ds\int_{\Delta}qp\sin^2(q,k)\,G(k,t',s)\,U(q,t,s)\,\Theta(p,t,s)\,dp\,dq, \quad t\geqslant t', \tag{A 3}$$

$$\left(\frac{\partial}{\partial t}+2\gamma k^2\right)\Theta(k,t,t)+2\int_{-\infty}^{t}\hat{\eta}(k,t,s)\,\Theta(k,s,t)\,ds=2\int_{-\infty}^{t}\langle f(\mathbf{k},t)f^*(\mathbf{k},s)\rangle\,G(k,t,s)\,ds$$
$$+2\pi k\int_{-\infty}^{t}ds\int_{\Delta}qp\sin^2(q,k)\,G(k,t,s)\,U(q,t,s)\,\Theta(p,t,s)\,dp\,dq, \tag{A 4}$$

with
$$\hat{\eta}(k,t,s)\equiv\pi k\int_{\Delta}pq\sin^2(q,k)\,G(p,t,s)\,U(q,t,s)\,dp\,dq, \tag{A 5}$$

where the Green's function, $G(\mathbf{k},t,s)$, represents the response of $\theta(\mathbf{k},t)$ to a unit perturbation [given by $f(\mathbf{k},s)$] in wave mode $\mathbf{k}$ at time s, where $U(k,t,t')$ and $\Theta(k,t,t')$ are the modal velocity and scalar variances defined in § 2, and where the integration domain for the magnitudes of the allowed wavenumbers is governed by the above triangle condition. The set (A 2)–(A 5) constitutes the Eulerian DIA equations which describe the temporal evolution of the scalar modal variances, $\Theta(k,t,t')$ and $\Theta(k,t,t)$, in isotropic turbulence assuming that the velocity modal variances are known [determined for example by the velocity field DIA equations given by Kraichnan (1964)]. The DIA turbulence model exhibits a number of desirable consistency properties (Kraichnan 1961) and accounts in a fundamental way for both nonlinear scrambling of energy and for stochastic relaxation of ensemble averages toward equilibrium.

The velocity field DIA equations provide fairly good predictions of low Reynolds number turbulence (Herring & Kraichnan 1972), but they yield unfaithful predictions of the inertial range of large Reynolds number turbulence. This improper behaviour of the DIA is attributed (Kraichnan 1964) to the fact that the DIA equations are not invariant to random Galilean transformations. Kraichnan (1965) rectified the inertial range problem of the DIA by developing the Galilean invariant Lagrangian history direct interaction approximation. This model provides good simulation of inertial range data. However, the model is quite complex, requiring significant amounts of computer time, and we have chosen not to use this statistical model for our predictions. Instead, we have utilized a test field model for isotropic scalar turbulence for our study of scalar decay. The TFM exhibits the Galilean invariance property, behaves properly in the inertial range and does not contain the temporal integrations, which are computationally costly, exhibited in the DIA and LHDIA equations. In addition, velocity field TFM simulations have been shown (Herring & Kraichnan 1972) to compare favourably with LHDIA simulations.

We develop our scalar TFM from the following Langevin representation of the scalar equation of motion; the random forcing is here specified to be white noise in time.†

$$\left(\frac{\partial}{\partial t}+\gamma k^2+\eta(k,t)\right)\theta(\mathbf{k},t) = Q(\mathbf{k},t)+f(\mathbf{k},t), \tag{A 6}$$

$$\eta(k,t) = \pi k\int_{\Delta} pq\sin^2(q,k)\,H(k,p,q)\,dp\,dq, \tag{A 7}$$

$$Q(\mathbf{k},t) = w(t)\sum_{\mathbf{k}=\mathbf{p}+\mathbf{q}}^{\Delta} i\mathbf{k}.N(\mathbf{q})\,\xi(\mathbf{p},t)\,[H(p,k,q)]^{\frac{1}{2}}, \tag{A 8}$$

where

$$\langle w(t)\,w(t')\rangle = \delta(t-t'),$$

$$\langle N_i(\mathbf{q})\,N_j(\mathbf{p})\rangle = \tfrac{1}{2}P_{ij}(\mathbf{q})\,\delta(\mathbf{p}+\mathbf{q}),$$

$$\langle f(\mathbf{k},t)f^*(\mathbf{k},t')\rangle = z(k,t)\,\delta(t-t'),$$

$$\langle\xi(\mathbf{p},t)\,\xi(\mathbf{q},t')\rangle = \langle\theta(\mathbf{p},t)\,\theta(\mathbf{q},t')\rangle = \Theta(p,t,t')\,\delta(\mathbf{p}+\mathbf{q}).$$

We assume that $\mathbf{N}(\mathbf{q})$ (a random, isotropic solenoidal vector), ξ, w and f are all statistically independent of each other and of the initial scalar field, $\theta(\mathbf{k}, 0)$. $H(k, p, q)$ is the triple moment scale which we define more explicitly below.

From (A 6) we find that the Green's function and time-displaced covariance function satisfy

$$\left(\frac{\partial}{\partial t}+\gamma k^2+\eta(k,t)\right)G_\theta(k,t,t') = 0 \quad (t\geqslant t'), \tag{A 9}$$

$$\left(\frac{\partial}{\partial t}+\gamma k^2+\eta(k,t)\right)\Theta(k,t,t') = 0 \quad (t\geqslant t'), \tag{A 10}$$

with

$$G_\theta(k,t',t') = 1. \tag{A 11}$$

Thus, $\Theta(k,t,t')$ and $G_\theta(k,t,t')$ obey the same differential equation and hence are proportional to one another (a statement of fluctuation–dissipation theory). Using (A 11) we obtain

$$\Theta(k,t,t') = G_\theta(k,t,t')\,\Theta(k,t',t'). \tag{A 12}$$

Also, from (A 6) we obtain the equation for the modal variance as

$$\left(\frac{d}{dt}+2\gamma k^2\right)\Theta(k,t,t)+2\eta(k,t)\,\Theta(k,t,t) = 2Z(k,t)+2\pi\int_{\Delta} pq\sin^2(q,k)\,H(p,k,q)\,\Theta(p,t,t)\,dp\,dq. \tag{A 13}$$

Comparing (A 13) with the DIA equation (A 4) [where we now set the initial time in (A 4) to zero and where we employ the Langevin model white noise form for the forcing function which transforms the integral forcing term to $2Z(k, t)$] we observe that we reproduce exactly the 'form' of the DIA equation with our model scalar variance equation if we define

$$H(p,k,q) = \int_0^t U(q,t,s)\,G_\theta(k,t,s)\frac{\Theta(p,t,s)}{\Theta(p,t,t)}\,ds. \tag{A 14}$$

† Our Langevin equation representation of the scalar equation of motion is modelled after a gradient-based, Markovian, Lagrangian history direct interaction scalar field representation proposed by Kraichnan (1970).

We note, however, that the Green's function for our model system will in general not equal the DIA Green's function. Employing (A 12) and an analogous Langevin model relation for the isotropic velocity field from Kraichnan (1971) we may write (A 14) as

$$H(p,k,q) = U(q,t,t)\int_0^t G_v(q,t,s)\,G_\theta(k,t,s)\,G_\theta(p,t,s)\,\frac{U(q,s,s)}{U(q,t,t)}\,\frac{\Theta(p,s,s)}{\Theta(p,t,t)}\,ds. \quad \text{(A 15)}$$

Now, following Kraichnan (1971), we define a new time scale (symmetric in p and k) in the light of (A 15) as

$$D^\theta(p,k,q) = \int_0^t G_v(q,t,s)\,G_\theta(k,t,s)\,G_\theta(p,t,s)\,ds, \quad \text{(A 16)}$$

and form a modified equation for $\Theta(k,t,t)$ as

$$\left(\frac{d}{dt}+2\gamma k^2\right)\Theta(k,t,t) = 2Z(k,t)+2\pi k\int_\Delta pq\sin^2(q,k)\,D^\theta(k,p,q)\,U(q,t,t) \times([\Theta(p,t,t)-\Theta(k,t,t)]\,dp\,dq. \quad \text{(A 17)}$$

Equation (A 17) reproduces exactly the form of the DIA equation (A 4) for the case of statistically steady scalar and velocity fields, so that the steady-state scalar-variance transfer exhibited by the DIA scalar model is reproduced by our Langevin scalar covariance equation. We adopt (A 17) as the basis for our TFM closure, although we must change the current choice of Green's functions in (A 16) to ensure that the Langevin model equations satisfy invariance under random Galilean transformations. $D^\theta(p,k,q)$ is a characteristic time scale for interactions between the wave modes k,p,q, and it represents the memory effects inherent in the DIA equations which result from the temporal integrations.

To complete the scalar model we note (after Kraichnan 1971) that the scalar gradient field is identically a compressive field since $\nabla\times(\nabla\theta)=0$ for every $(\mathbf{x},t)$, and thus we shall view the scalar-gradient field as a test field.We next associate the Green's function of the compressive velocity test field developed by Kraichnan (1971) with our scalar Green's function G_θ, and further associate the solenoidal Green's function of Kraichnan (1971) with the Langevin model velocity Green's function, G_v. If we now substitute the compressive and solenoidal test field Green's function into (A 16), after rescaling Kraichnan's (1971) test field motion equations so that the relaxation time for the scalar variance is $\eta^c(k)\,g_\theta$ (with the notation given in § 2), and differentiate we obtain

$$dD^\theta(k,p,q)/dt = 1-(g_\theta^2(\eta^c(k)+\eta^c(p))+\eta^s(q)+\gamma(k^2+p^2)+\nu q^2)\,D^\theta(k,p,q), \quad \text{(A 18)}$$

with $$D^\theta(k,p,q|t=0)=0.$$

The set (A 10), (A 17) and (A 18) comprise the scalar TFM employed for this work which has been given in § 2. We now record consistency properties of the scalar TFM.

The scalar TFM equations satisfy invariance to random Galilean transformations because of the replacement of the Green's functions in (A 16) with the solenoidal and compressive test field Green's functions. Further, the test field Green's functions are positive, monotonic decreasing functions of t (Kraichnan 1971) so that (A 16) ensures that $D^\theta(k,p,q)\geqslant 0$ for every t; an essential quality in view of our Langevin equation (A 8). In addition, the scalar TFM may be shown to satisfy conservation of

scalar variance by nonlinear interaction [(3.8)] by forming $T_\theta(k)$ from (A 17) and then utilizing both the symmetry in k and p of $D^\theta(k, p, q)$ and the symmetry of the integration domain described in § 3.

The existence of the model scalar Langevin system ensures that the scalar TFM yields realizability of the modal scalar variance, $\theta(k, t, t)$. In addition, the scalar TFM is consistent with the inviscid equipartitioning behaviour which can be exhibited from a truncated wavenumber representation of the scalar equation of motion. We see from (A 17) that, with zero forcing and with $\gamma = 0$, if our TFM system achieves $\Theta(k, t, t) =$ constant for every k at some t_1, then (A 17) ensures $\Theta(k, t, t) =$ constant for every $t > t_1$ providing the velocity field has also achieved equipartition equilibrium. We note further that the forms of the 'input' and 'drain' terms of the TFM modal variance equation, (A 17), are consistent with a tendency for equipartitioning. The terms act to drain modal variance from wavenumber regions with excess variance and input variance into wavenumbers exhibiting modal variance deficiencies. Finally, we note that numerical studies [described by Orzsag (1974)] of isotropic turbulence with an eddy-damped Markovian model have shown that the simulated velocity field tends towards modal energy equipartition. Since the scalar TFM equation for $\Theta(k, t, t)$ has exactly the 'input' and 'drain' forms of the Markovian equation for $U(k, t, t)$, we infer that the scalar TFM system would exhibit similar equipartitioning behaviour.

REFERENCES

Batchelor, G. H., Howells, I. D. & Townsend, A. 1959 Small scale variation of convected quantities like temperature in turbulent fluid. *J. Fluid Mech.* **5**, 134.

Champagne, F. H., Friehe, C. A., la Rue, J. C. & Wyngaard, J. C. 1977 Flux measurements, flux estimation techniques, and fine-scale turbulence measurements in the unstable surface layer over land. *J. Atmos. Sci.* **34**, 515.

Clay, J. P. 1973 Turbulent mixing of temperature in water, air, and mercury. Ph.D. dissertation in Engineering Sci. (Engr. Phys.), University of California at San Diego.

Gibson, C. H. 1962 Scalar mixing in turbulent flow. Ph.D. thesis, Stanford University.

Gibson, C. H. 1968 Fine structure of scalar fields mixed by turbulence. II. Spectral theory. *Phys. Fluids* **11**, 2316.

Grant, H. L., Hughes, B. A., Vogel, W. M. & Moilliet, A. 1968 The spectrum of temperature fluctuations in turbulent flow. *J. Fluid Mech.* **34**, 423.

Grant, H. L., Stewart, R. W. & Moilliet, A. 1962 Turbulence spectra from a tidal channel. *J. Fluid Mech.* **12**, 241.

Herring, J. R. & Kraichnan, R. H. 1972 Comparison of some approximations for isotropic turbulence. *Statistical Models and Turbulence*, p. 148. Berlin: Springer-Verlag.

Kraichnan, R. H. 1959 The structure of isotropic turbulence at very high Reynolds numbers. *J. Fluid Mech.* **5**, 447.

Kraichnan, R. H. 1961 Dynamics of nonlinear stochastic systems. *J. Math. Phys.* **2**, 124.

Kraichnan, R. H. 1964 Decay of isotropic turbulence in the Direct Interaction Approximation. *Phys. Fluids* **7**, 1030.

Kraichnan, R. H. 1965 Lagrangian history closure approximation for turbulence. *Phys. Fluids* **8**, 575.

Kraichnan, R. H. 1966 Isotropic turbulence and inertial range structure. *Phys. Fluids* **9**, 1778.

Kraichnan, R. H. 1968 Small scale structure convected by turbulence. *Phys. Fluids* **9**, 1728.

Kraichnan, R. H. 1970 Notes on Lagrangian history amplitude models. Private communication, J. R. Herring.

KRAICHNAN, R. H. 1971 An almost-Markovian Galilean-invariant turbulence model. *J. Fluid Mech.* **47**, 513.

LEITH, C. E. 1968 Diffusion approximation for turbulent scalar field. *Phys. Fluids* **11**, 1612.

LEITH, C. E. & KRAICHNAN, R. H. 1972 Predictability of turbulent flows. *J. Atmos. Sci.* **29**, 1041.

LESIEUR, M. & SCHERTZER, D. 1978 Dynamique des gros Tourbillons et Décroissance de L'énergie Cinétique en Turbulence Tridimensionelle Isotope à Grand Nombre de Reynolds. *J. Méc.* **225**, 464.

LIN, S.-C. & LIN, S.-C. 1973 Study of strong temperature mixing in subsonic grid turbulence. *Phys. Fluids.* **16**, 1587.

LUMLEY, J. L. 1970 Toward a turbulent constitutive relation. *J. Fluid Mech.* **41**, 413.

LUMLEY, J. L. & NEWMAN, G. R. 1977 The return of isotropy of homogeneous turbulence. *J. Fluid Mech.* **82**, 161.

MONIN, A. S. & YAGLOM, A. M. 1975 *Statistical Fluid Mechanics*, vol. 2. Cambridge, Mass.: MIT Press.

NEWMAN, G. R., LAUNDER, B. E. & LUMLEY, J. L. 1979 Modelling the behaviour of homogeneous scalar turbulence. To be submitted to *J. Fluid Mech.*

ORSZAG, S. A. 1974 Lectures on the statistical theory of turbulence. *Flow Research Report*, no. 31.

SCHUMANN, U. 1977 Realizability of Reynolds stress turbulence models. *Phys. Fluids* **20**, 721.

UBEROI, M. S. 1963 Energy transfer in isotropic turbulence. *Phys. Fluids* **6**, 1048.

VAN ATTA, C. W. & CHEN, W. Y. 1969 Measurements of spectral energy transfer in grid turbulence. *J. Fluid Mech.* **38**, 743.

WARHAFT, Z. & LUMLEY, J. L. 1978 An experimental study of the decay of temperature fluctuations in grid-generated turbulence. *J. Fluid Mech.* **88**, 659.

WILLIAMS, R. M. 1974 High frequency temperature and velocity fluctuations in the atmospheric boundary layer. Ph.D. thesis, Oregon State University, Corvallis.

YEH, T. T. & VAN ATTA, C. W. 1973 Spectral transfer of scalar and velocity fields in heated-grid turbulence. *J. Fluid Mech.* **58**, 233.